Novel Mechanism whereby Metformin Improves Glucose Homeostasis: TXNIP-GLUT1 Axis Modulation Enhances Intestinal Glucotonic Effects

Nam, Jung Ho

Department of Medical Science
Graduate School
Yonsei University

Novel Mechanism whereby Metformin Improves Glucose Homeostasis: TXNIP-GLUT1 Axis Modulation Enhances Intestinal Glucotonic Effects

Advisor Sung Soon Fang

A Dissertation Submitted
to the Department of Medical Science
and the Committee on Graduate School of Yonsei University
in Partial Fulfillment of the
Requirements for the Degree of
Doctor of Philosophy in Medical Science

Nam, Jung Ho

July 2025

This certifies that the Dissertation of Jung Ho Nam is approved

Thesis Supervisor	Sung Soon Fang
Thesis Committee Member	Eun Jig Lee
Thesis Committee Member	Cheol Ryong Ku
Thesis Committee Member	Yong-ho Lee
Thesis Committee Member	Chang-Myung Oh

The Graduate School
Yonsei University

July 2025

ACKNOWLEDGEMENTS

Firstly, I would like to express my sincere gratitude to my advisor, Prof. Eun Jig Lee, for his continuous support throughout my Ph.D. studies. His passion for research, encouragement, and motivation have been invaluable to me. Without his guidance and support, I would not have been able to embark on this research journey. I am also grateful to my thesis supervisor, Prof. Sung Soon Fang, whose insightful advice and keen interest have been instrumental in the successful completion of this dissertation.

Above all, I would like to extend my deepest gratitude to Prof. Cheol Ryong Ku. His exceptional guidance and unwavering support have been invaluable throughout my academic journey. I am truly grateful for the opportunity to be part of his research group, where I was fortunate to work alongside incredible colleagues and conduct meaningful experiments. His mentorship has not only shaped my research but also inspired me to strive for excellence. Without his continuous encouragement and dedication, this dissertation would not have been possible.

I would like to extend my appreciation to the rest of my thesis committee: Prof. Yong-ho Lee, and Prof. Chang-Myung Oh for their valuable feedback and guidance. Their diverse perspectives have greatly contributed to the depth of my research.

My sincere thanks also go to my mentor, Dr. Chan Woo Kang, for his invaluable teachings, profound advice, and unwavering support. His mentorship has played a significant role in shaping my academic journey.

I am truly grateful to my fellow researchers Dr. Yang Jong Lee, Dr. Ju Hun Oh, Eun Kyung Wang, Soo Hyun Lee, Hye Ju Shin, and Ye Bin Kim. It has been an honor to work alongside them, and I cherish the experiences we have shared.

Lastly, I would like to express my heartfelt gratitude to my family: my future wife, my parents: Dr. Jae Hyun Nam, Jung Lim Choi and my sister: Dr. Jung Eun Nam. Without their patience and unwavering support, this achievement would not have been possible. Their endless love and encouragement have been my greatest source of strength, and I want to take this moment to say that I will always love and cherish them.

TABLE OF CONTENTS

LIST OF FIGURES

ABSTRACT

Novel Mechanism whereby Metformin Improves Glucose Homeostasis: TXNIP-GLUT1 Axis Modulation Enhances Intestinal Glucotonic Effects

Metformin is widely used as a first-line therapy for type 2 diabetes mellitus however, the molecular mechanisms by which it modulates intestinal glucose metabolism remain incompletely defined. Metformin was orally administered to male C57BL/6 mice, followed by IPGTT and 18F-FDG tracing to evaluate glucose homeostasis. To investigate changes in intestinal glucose metabolism, IEC-6 and Caco-2 cell lines were used for in vitro analysis, with organoid experiments conducted for further validation. qRT-PCR, western blotting, flow cytometry, and immunohistochemistry were performed to elucidate the effects of metformin on glucose metabolism pathways. Metformin enhanced glucose uptake and excretion in the distal intestine, particularly in the ileum and colon. Mechanistically, metformin upregulated the expression and membrane localization of glucose transporter 1 (GLUT1) by downregulating thioredoxin-interacting protein (TXNIP) expression. Consistently, intestinal-specific overexpression of TXNIP abolished metformin-induced improvements in glucose tolerance, while pharmacological inhibition of GLUT1 similarly negated metformin's glucose-lowering effects. Our findings identified intestinal glucose excretion, mediated through the intestinal TXNIP-GLUT1 regulatory axis, as a previously unrecognized contributor to metformin's glucoregulatory action. These results highlight a novel intestinal mechanism underlying metformin's efficacy and provide insights for potential therapeutic strategies beyond traditional glucose regulation.

Key words : glucose homeostasis; metformin; GLUT1; gastrointestinal tract; TXNIP

1. Introduction

Type 2 diabetes and metabolic diseases are among the most prevalent health disorders in modern society, with a recent increase in the number of in-patient cases. Researchers have extensively studied metformin for its diverse pharmacological actions[1-3]. Researchers have proposed various functional mechanisms for metformin effects, and they regard the involvement of 5′-AMP-activated protein kinase (AMPK)-dependent pathways as pivotal[4-7]. Despite over six decades of clinical application and extensive research, the precise mode of action of metformin remains unclear.

Previous research focused on elucidating the glucose-lowering mechanisms of metformin in the adipose tissue, muscle, and liver of diabetic models[8,9]. However, researchers lack a comprehensive understanding of its broad-spectrum glucose-lowering effects, including in non-disease models. Recent research has focused on the metabolic role of the intestine via exploring incretins, such as GLP-1[10,11], microbiome[12,13], and gut-derived peptides[10,14]. The potential metabolic benefits of metformin, attributed to its action in the intestine, have also been highlighted. Studies have reported a significant increase in metformin biodistribution in the intestine following oral administration[15].

The solute carrier family 2 (SLC2) proteins or glucose transporters (GLUTs) are responsible for passive glucose transport across cell membranes[16]. Among them, GLUT1 (SLC2A1) is ubiquitously expressed and mediates basal glucose uptake in various tissues, including the intestine[17,18]. GLUT1 activity is closely regulated by its expression levels and membrane localization, both of which respond dynamically to cellular energy demand and metabolic stress.

Thioredoxin-interacting protein (TXNIP), a redox-sensitive regulator, binds and inhibits thioredoxin, thereby promoting oxidative stress and increasing intracellular reactive oxygen species (ROS)[19]. TXNIP expression is induced under hyperglycemic or oxidative conditions and has been implicated in insulin resistance, β-cell dysfunction, and

impaired glucose homeostasis[20-22]. Importantly, TXNIP negatively regulates glucose uptake by reducing membrane GLUT1 localization through internalization and degradation mechanisms [23,24]. While the GLUT1–TXNIP regulatory axis has been explored in various metabolic tissues, its role in the intestinal epithelium, especially in the context of metformin action, remains poorly defined.

Advanced imaging techniques such as positron emission tomography–computed tomography (PET–CT), have revealed that metformin stimulates intestinal glucose uptake [25,26]. Moreover, bariatric procedures, such as Roux-en-Y gastric bypass (RYGB), enhance both intestinal glucose uptake and intraluminal glucose excretion, suggesting a dual role of the gut in systemic glucose regulation [27-29]. Although metformin influences intestinal glucose metabolism, most studies have focused on its uptake-promoting effects, and little is known about the mechanistic relevance of these changes in clinical glucose control.

In this study, we investigated the contribution of intestinal glucose handling to metformin's systemic metabolic effects. Specifically, we identified the GLUT1–TXNIP axis as a key molecular pathway mediating metformin-induced alterations in intestinal glucose metabolism and propose that this mechanism plays a critical role in its glucose-lowering effect.

2. METERIALS AND METHODS

2.1. Animal experiments

After a 1-week acclimatization period, male C57BL/6 mice were orally gavaged with 150 mg/kg of metformin. Following a 6 h fasting period, 18F-FDG injection was performed to trace glucose uptake. Metformin was orally administered at a dose of 150 mg/kg 2 h prior to FDG injection. One-hour post-FDG injection, mice were euthanized, and the intestines were excised en bloc. Limbs were flushed with phosphate-buffered saline (PBS), and PBS washings were collected for gamma counting to quantify fecal FDG excretion. Autoradiography images of the post-wash intestines were obtained to identify areas of high glycolytic rates within the intestinal wall. Similar experimental methods were employed to evaluate the glucose homeostasis effect of GLUT1 inhibition in metformin-treated mice. Following a 1-week acclimatization period, mice were intraperitoneally injected with STF-31 (GLUT1-specific inhibitor) at a dose of 7.8 mg/kg once daily for 3 days. Three days later, mice received oral gavage of metformin at 150 mg/kg followed by injection of STF-31. Glucose homeostasis was assessed through an IPGTT with 2.5 g/kg glucose. The following day, mice received the same treatment of metformin and STF-31, followed by FDG injection and sacrifice, with subsequent sampling conducted as previously described. Our study examined male mice because male animals exhibited less variability in phenotype. All animal handling procedures adhered to the guidelines established by Association for Assessment and Accreditation of Laboratory Animal Care International and were approved by Yonsei University Institutional Animal Care and Use Committee.

2.2. Establishment of the TXNIP overexpressed diabetic animal model

C57BL/6, male mice were used in healthy mouse experiments or were rendered diabetic by multiple low dose STZ injections (3 days; IP injection; freshly prepared in 0.1

mmol/L sodium citrate at pH 4.5). Five days after the first STZ injection according to the in vivo transfection protocol (invivo-jetPEI, Polyplus, Berkeley, CA, USA), mice were subjected to tail vein injection of TXNIP. After TXNIP injection, metformin at a dose of 250 mg/kg was administered via oral gavage. On the fourth day of metformin treatment, an intraperitoneal glucose tolerance test (IPGTT) was conducted. The following day, after administering metformin, mice were injected with 18F-fluorodeoxyglucose (FDG) and sacrificed 1 h later for further analysis. The fasting duration and the time intervals between metformin gavage and subsequent procedures on the IPGTT day, as well as on the FDG injection measurement day, were the same as in the previous metformin experiment.

2.3. Cell culture

IEC-6 cells were maintained at 37 °C under 5% CO_2 in Dulbecco's modified Eagle's medium (Cytiva, Marlborough, MA, USA) supplemented with 10% fetal bovine serum (FBS) and 1% penicillin-streptomycin. Caco-2 cells were grown in Minimal Essential Medium with Earle's Balanced Salts (Cytiva, Marlborough, MA, USA) medium supplemented with 10% fetal bovine serum (FBS) and 1% penicillin-streptomycin and 25 mM HEPES.

2.4. Crypt isolation and culture for organoid studies

Crypt isolation and culture for organoid studies the small intestines of C57BL/6J mice were harvested. The fat and villi were removed, and the samples were incubated at 4 °C for 15 min to isolate the crypts. After passing the crypt suspension through a cell strainer and centrifugation, 50–200 crypts were suspended in 25 μL of Matrigel (BD Biosciences, San Jose, CA, USA). From the isolation of intestinal crypt organoids to their maintenance and subsequent seeding into a monolayer for experimental use, procedures were conducted following protocols outlined in stem cell technology literature.

2.5. Electroporation

After a 1-week acclimatization Cells were harvested at a density of 1×10^6 cells and mixed with plasmid diluted in Opti-MEM reduced serum media (Thermo Fisher Scientific, Waltham, MA, USA). Transfection was achieved through electroporation using the NEPA21 system following the electroporation protocol.

2.6. Histology and immunostaining

Intestinal tissues from the animal models were paraffin-embedded and sectioned. Tissue sections (4 μm thick) were cut from each block for either H&E staining or immunostaining with the following antibodies: rabbit anti-GLUT1 (Abcam, Cambridge, MA, USA), rabbit anti-TXNIP (Abcam, Cambridge, MA, USA,).

2.7. RNA purification and quantitative PCR

Total RNA was isolated from cells and tissues using RNeasy Mini purification kit (Qiagen, Maryland, MD, USA) according to the manufactures protocol. Tissues were homogenized in RLT buffer using a bead homogenizer for 3 min at max speed (Qiagen, TissueLyser II). cDNA was prepared using ReverTra Ace (Toyobo, Osaka, Japan) according to the manufacturer's instructions. The resulting cDNA was subjected to quantitative real-time PCR using the Power SYBR Green PCR Master Mix (Applied Biosystems) according to the manufacturers' instructions. The primers and sequences used are listed in the table.

2.8. Western blot analysis

Cells were washed in ice-cold PBS and lysed on ice using cell lysis buffer (Cell Signaling Technology, Beverly, MA, USA) for total cellular protein. Tissues were homogenized and lysed in T-per Tissue protein extraction reagent (Thermo Fisher Scientific, Waltham, MA, USA) using a bead homogenizer for 3 min at max speed (Qiagen,

TissueLyser II) for total tissue protein. Membrane-and-cytoplasmic protein fractions of cultured cells and tissue were obtained with Mem-PER Plus Membrane Protein Extraction Kit (Pierce Protein Biology) for membrane cellular and tissue protein. Each lysate was supplemented with Protease inhibitor Cocktail (Sigma-Aldrich, St. Louis, MO, USA) and Phosphatase Inhibitor Cocktail 2 (Sigma-Aldrich, St. Louis, MO, USA) and Phosphatase Inhibitor Cocktail 3 (Sigma-Aldrich, St. Louis, MO, USA). Lysates were centrifuged at 16,000 rpm for 15 min at 4 °C and protein concentrations were quantified using BCA Protein Assay Kit (Sigma-Aldrich, St. Louis, MO, USA). Equal amounts of lysate were mixed with NuPAGE LDS Sample Buffer (4X) (Thermo Fisher Scientific, Waltham, MA, USA) and boiled for 10 min at 70 °C before being subjected to electrophoresis in NuPAGE 4–12% Bis-Tris Protein Gels (Thermo Fisher Scientific, Waltham, MA, USA). Proteins were resolved on 4%–20% gradient SDS-PAGE, transferred to PVDF membranes and probed with antibodies for GLUT1 (Abcam, Cambridge, MA, USA), TXNIP (Cell Signaling Technology, Beverly, MA, USA), GLUT2(Novus, NBP2-22218), SGLT1 (Novus, NBP2-20338), B-actin (Santa Cruz, sc-47778), Na^+/K^+-ATPase (ATP1A1) (Abcam, Cambridge, MA, USA).

2.9. 2DG uptake assay

2DG uptake is performed according to the procedure described in the Glucose-Uptake-Glo Assay kit (Promega). Glucose uptake is processed for 60 min and is divided into 3 or 4 parts. Fluorescence was measured 60 min after treatment with 2-deoxyglucose 6-phosphate using GloMax discover (Promega).

2.10. Glucose excretion

Cells were seeded in the upper wells of transwell inserts and allowed to form a monolayer. Following 16 h of treatment with metformin, the upper wells were supplemented with high glucose media, while the lower wells received no glucose media. After 30 min, glucose transport across the membrane was assessed using Glucose

Colorimetric Detection. To confirm whether glucose diffusion into the lower well occurred solely through passive diffusion or via cellular transport, dextran was utilized.

2.11. Flow cytometry

Cells from in vitro experiments were collected on ice in 10 mM EDTA in PBS and fixed with 4% paraformaldehyde prior to flow cytometric analysis. Cells were incubated with 1:100 anti-rabbit GLUT1(Abcam, Cambridge, MA, USA) antibody in BD Stain Buffer (BSA) (BD Biosciences) 30 min in RT after 20 min on ice to block non-specific binding, followed by incubation for 30 min on RT with 1:200 Alexa Fluor 647(Abcam, Cambridge, MA, USA). Cells were rinsed twice and then resuspended in fresh buffer for analysis on a BD FACS verse II flow cytometer using BD FACS Diva software (BD Biosciences).

2.12. Immunocytochemistry

For intestinal organoids cultured on coverslips were washed with ice-cold PBS and fixed in 4% paraformaldehyde. The organoids were then incubated with anti-GLUT1 (1:500; ab115730, Abcam) for 12 h, followed by Alexa Fluor-488-conjugated rabbit, and Flash Phalloidin Red-594 (1:100, 424203, Biolegend ,San Diego, CA, USA) for 1 h. Finally, the coverslips were mounted in Vectashield (Vector Laboratories, Burlingame, CA, USA) and examined using a confocal laser-scanning microscope (Zeiss LSM780; Carl Zeiss MicroImaging, Thornwood, NY, USA).

2.13. RNA sequencing

Total RNA concentration was calculated by Quant-IT RiboGreen (Invitrogen, Carlsbad, CA, USA). To assess the integrity of the total RNA, samples are run on the TapeStation RNA screentape (Agilent, Santa Clara, CA, USA). Only high-quality RNA preparations with RIN greater than 7.0, were used for RNA library construction.

A library was independently prepared with 0.5 μg of total RNA for each sample by Illumina TruSeq Stranded Total RNA Library Prep Gold Kit (Illumina, Inc., San Diego, CA, USA). The first step in the workflow involves removing the rRNA in the total RNA. Following this step, the remaining mRNA is fragmented into small pieces using divalent cations under elevated temperature. The cleaved RNA fragments are copied into first strand cDNA using SuperScript II reverse transcriptase (Invitrogen, #18064014) and random primers.

This is followed by second strand cDNA synthesis using DNA Polymerase I, RNase H and dUTP. These cDNA fragments then go through an end repair process, with the addition of a single 'A' base, and then ligation of the adapters. The products are then purified and enriched with PCR to create the final cDNA library.

The libraries were quantified using KAPA Library Quantification kits for Illumina Sequencing platforms according to the qPCR Quantification Protocol Guide (KAPA BIOSYSTEMS, #KK4854) and qualified using the TapeStation D1000 ScreenTape (Agilent Technologies, # 5067-5582). Indexed libraries were then submitted to an Illumina NovaSeq (Illumina, Inc., San Diego, CA, USA), and the paired-end (2×100 bp) sequencing was performed by Macrogen Incorporated.

2.14. Data processing and analysis

Paired-end sequencing reads were generated on the Illumina sequencing NovaSeq platform. Before starting the analysis, Trimmomatic v0.38 was used to remove adapter sequences and trim bases with poor base quality. The cleaned reads were aligned to the Mus musculus (mm10) using HISAT v2.1.0 (KIM et al, 2015), based on the HISAT and Bowtie2 implementations. The reference genome sequence and gene annotation data were downloaded from the NCBI Genome assembly and NCBI RefSeq database respectively. Aligned data (SAM file format) were sorted and indexed using SAMtools v 1.9. After alignment, the transcripts were assembled and quantified using StringTie v2.1.3b (Pertea, Mihaela, et al., 2015, 2016). Gene-level and Transcript-level quantification were calculated

as raw read count, FPKM (Fragments Per Kilobase of transcript per Million mapped reads), and TPM (Transcripts Per Million).

2.15. Differential gene expression analysis

The relative abundances of gene were measured in FPKM (Fragments Per Kilobase of exon per Million fragments mapped) using StringTie [30-33]. We performed the statistical analysis to find differentially expressed genes using the estimates of abundances for each gene in samples. Genes with one more than zeroed FPKM values in the samples were excluded. To facilitate log2 transformation, 1 was added to each FPKM value of filtered genes. Filtered data were log2-transformed and subjected to quantile normalization. Statistical significance of the differential expression data was determined using an independent t-test and fold change in which the null hypothesis was that no difference exists among groups. False discovery rate (FDR) was controlled by adjusting p value using Benjamini-Hochberg algorithm. For the DEG set, hierarchical clustering analysis was performed using complete linkage and Euclidean distance as a measure of similarity. Gene-enrichment and functional annotation analysis and pathway analysis for significant gene lists were performed based on Gene Ontology (www.geneontology.org/). All data analysis and visualization of differentially expressed genes was conducted using R 3.6.1 (www.r-project.org). The data discussed in this publication have been deposited in NCBI's Gene Expression Omnibus (Edgar et al., 2002) and are accessible through GEO Series accession number GSE271623.

2.16. Quantification and statistical analysis

All data in the current study were represented as mean ± SEM with the numbers of experiments or mice indicted in the Figure legends. Unpaired two-tailed Student's t-test was used for the comparisons between two groups. Differences between multiple groups with one variable were determined using multiple t-test. Statistical analyses performed using the GraphPad Prism 6 software. Significance was defined as $*P < 0.05$, $**P < 0.01$,

***P < 0.001 and #P < 0.05, ##P < 0.01. No method was used to determine whether the data met the assumptions of the statistical approach. A power analysis was not performed to determine the sample size.

3. RESULTS

3.1. Metformin enhances glucose uptake and excretion in the distal intestine

To determine the effect of metformin on glucose regulation, we examined the effect of a single dose of metformin in C57BL/6 mice and compared the results with those obtained in vehicle-treated mice. intraperitoneal glucose tolerance test (IPGTT) was performed to compare the initial responses of glucose metabolism. Metformin-treated mice exhibited enhanced blood glucose homeostasis compared with that of vehicle-treated mice (Figure 1A). To determine specific location of the gastrointestinal (GI) tract where metformin regulates glucose metabolism, the entire gastrointestinal tract of mice was subjected to autoradiography using 2-deoxy-2-[18F]-fluoro-D-glucose (18F-FDG) as a glucose tracer. A significant increase in glucose uptake was observed in the distal intestine of metformin-treated mice compared with that in vehicle-treated mice (Figure 1B). Analysis of 18F-FDG gamma counts revealed that compared with the vehicle-treated group, the metformin-treated group exhibited higher glucose uptake in the ileum and colon than in the proximal intestine (Figure 1C). Furthermore, FDG excretion was significantly increased in the stool of metformin-treated mice compared to that in vehicle-treated mice (Figure 1D). These results suggest that the increased glucose uptake and excretion (glucotonic effect) in the distal intestine and colon following metformin administration indicate that metformin acts at these regions to exert its blood glucose-lowering effects.

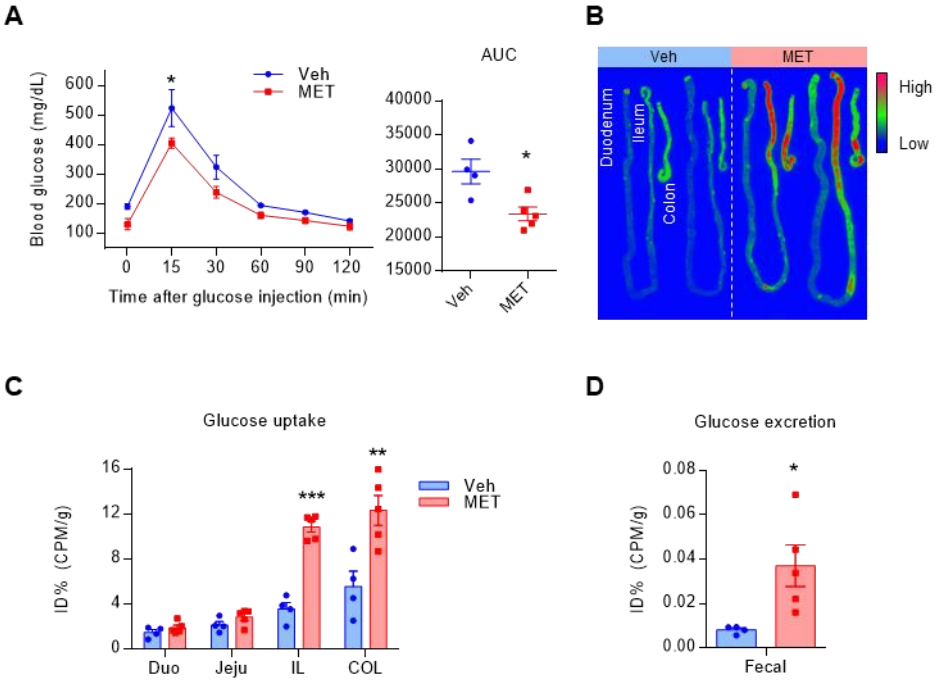

Figure 1. Metformin enhances blood glucose homeostasis by increasing glucotonic effect in the distal intestine and colon of C57BL/6 mice. Metformin increases glucose homeostasis and intestinal glucotonic effect. (**A**) IPGTT data for vehicle (saline) and metformin treated mice. Metformin-treated (MET) C57BL/6 mice (n=4) exhibited better glucose tolerance than vehicle-treated (Veh) mice (n=4, analysis of variance multiple t-test for multiple comparison correction) and corresponding area under the curve (AUC). (**B**) Representative images of small intestinal and colon 2-Deoxy-2-[18F]-fluoro-D-glucose (FDG) autoradiography of Metformin-treated and vehicle-treated mice after PBS lavage. Areas of higher FDG accumulation are red in colour. (**C**) The graph shows the quantitative analysis of FDG uptake in the post-washing intestine tissue autography images. Metformin-treated limbs showed higher FDG uptake in the distal intestine, such as the ileum (IL) and colon (COL), compared with that in the corresponding vehicle-treated intestine, whereas no increase was observed in the proximal intestine, such as the duodenum (DUO) and jejunum (JEJU). (**D**) Colon phosphate buffered saline (PBS) washing analysis. Colon PBS

washings showed larger amount of FDG excretion in the metformin-treated mice. All data are presented as the mean ± SEM. Data in A, C, and D were analyzed using two-tailed Student's t-tests; *P < 0.05, **P < 0.01, ***P < 0.001.

3.2. Metformin enhances GLUT1 expression and function in intestinal cells

Previous studies have demonstrated that changes in glucose metabolism within the GI tract observed following gastric bypass surgery or metformin treatment are associated with alterations in the gene expression of glucose transporters[26,28,34-36]. To identify the specific glucose transporters that play a major role in the glucotonic effect induced by metformin, mRNA levels of multiple glucose transporters were examined using both rat ileum (IEC6) and human colon (Caco-2) cell lines. Both cell lines exhibited significantly increased expression of GLUT1 (Figure 2A). Moreover, both cell lines also showed a significant increase in the expression of hexokinase 2 (HK2), which enables the measurement of glycolysis following glucose transport into the cell via the glucose transporter[37]. In contrast, all other transporters showed no significant change in transcript levels in IEC6 cells. However, GLUT2 and GLUT5 expression was reduced in Caco-2 cells following metformin treatment, with no significant changes observed in the other transporters (Figure 2A). Unlike the glycolysis-related enzyme HK2, the gluconeogenesis-related enzymes phosphoenolpyruvate carboxykinase 1 (PCK1) and glucose-6-phosphatase catalytic subunit (G6PC) exhibited no consistent changes, indicating no common effect on gluconeogenesis in both IEC6 and Caco-2 cells. Notably, only PCK1 levels increased significantly in Caco-2 cells. In addition, treatment with phenformin, another biguanide, mirrored the effects of metformin, significantly increasing GLUT1 and HK2 mRNA expression in both cell lines (Figure 2B). Consistently, treatment with biguanides (metformin, phenformin, and buformin) resulted in increased GLUT1 protein expression in both IEC6 and Caco-2 cell lines (Figure 2C). Since active GLUT1 primarily localizes to the cell membrane and facilitates glucose transport across the cell membrane[17],

we extracted membranous proteins from IEC6 and Caco-2 cells and measured GLUT1 activity after treatment with metformin or phenformin. Membranous GLUT1 levels significantly increased following metformin and phenformin treatment in both cell lines (Figure 2D). Although the protein levels of GLUT2 and SGLT1, intestinal glucose transporters[18,38], showed no changes in Caco-2 cells, they increased in IEC6 cells. However, there were no significant changes in membrane proteins in either cell line after metformin treatment (Figure 2E and 2F). Next, mouse intestinal and colorectal organoids were established to investigate the effects of metformin in a setting mirroring in vivo. GLUT1 expression was significantly increased in the plasma membranes of metformin-treated intestinal and colorectal organoids (Figure 2G). These results suggested that metformin induces glycolysis by increasing GLUT1 expression and membrane translocation in the distal intestine. Furthermore, 2DG uptake assay revealed that metformin treatment increased glucose uptake in both intestinal cell lines (Figure 2H). To determine the involvement of GLUT1 in mediating this effect, cells were treated with STF-31, a GLUT1-specific inhibitor[39,40], in combination with metformin. STF-31 treatment abolished the metformin-induced increase in glucose uptake in both cell lines, confirming the role of GLUT1 in this process (Figure 2H). Moreover, metformin treatment enhanced glucose excretion in both the IEC6 and Caco-2 cell lines (Figure 2I). Notably, the diffusion of FITC-dextran was not observed, confirming that the excreted glucose was not the result of diffusion, but occurred via the glucose transporter (Figure 2J). Moreover, STF-31 treatment abolished the metformin-induced glucose excretion in both cell lines (Figure 2I). To replicate and verify whether glucose secretion induced by metformin in organoids, we measured the amount of glucose in the media from monolayer-seeded colon organoids. Glucose secretion was significantly increased in metformin-treated colon organoids (Figure 2K). These results highlight the crucial role of GLUT1 in metformin-induced increases in intestinal glucotonic effect.

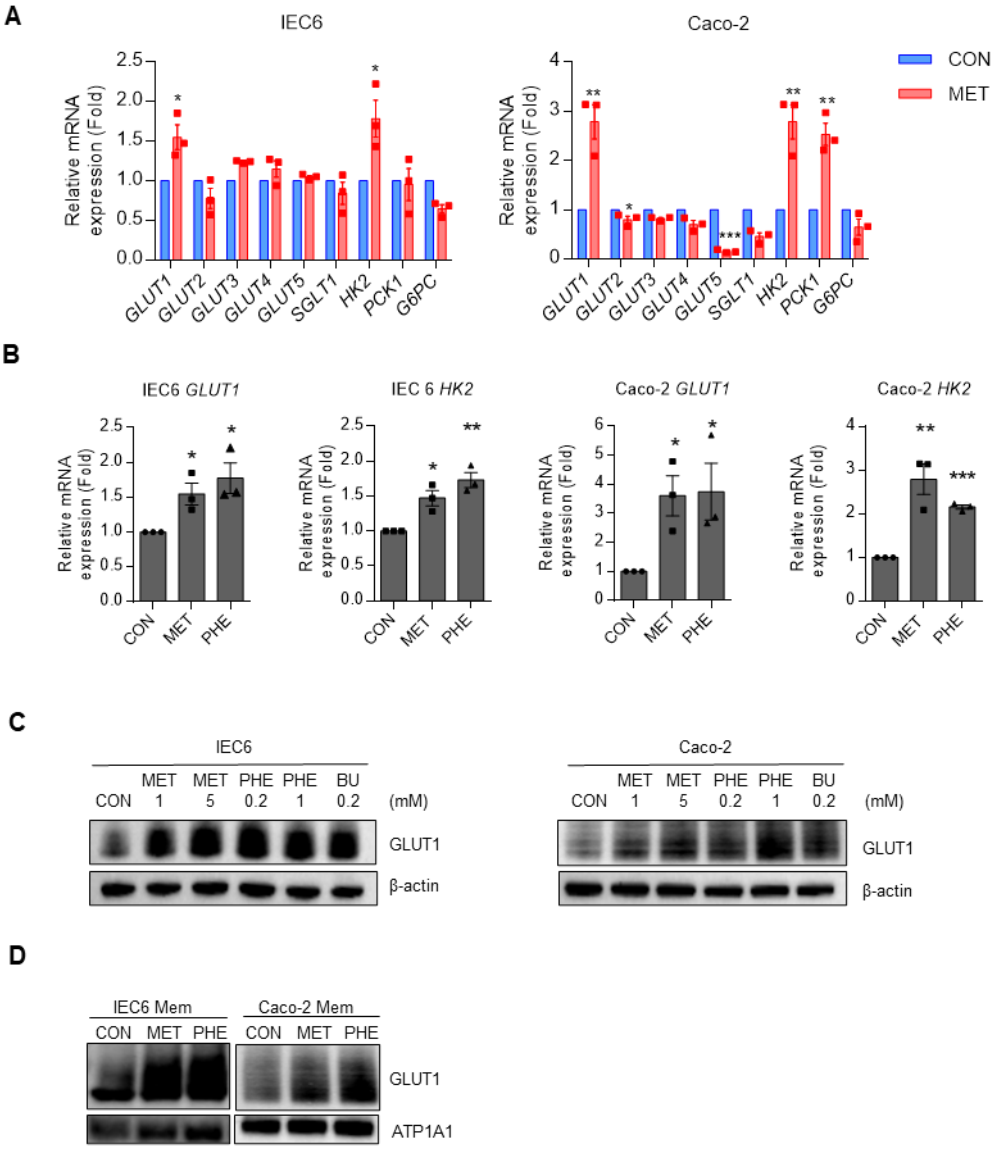

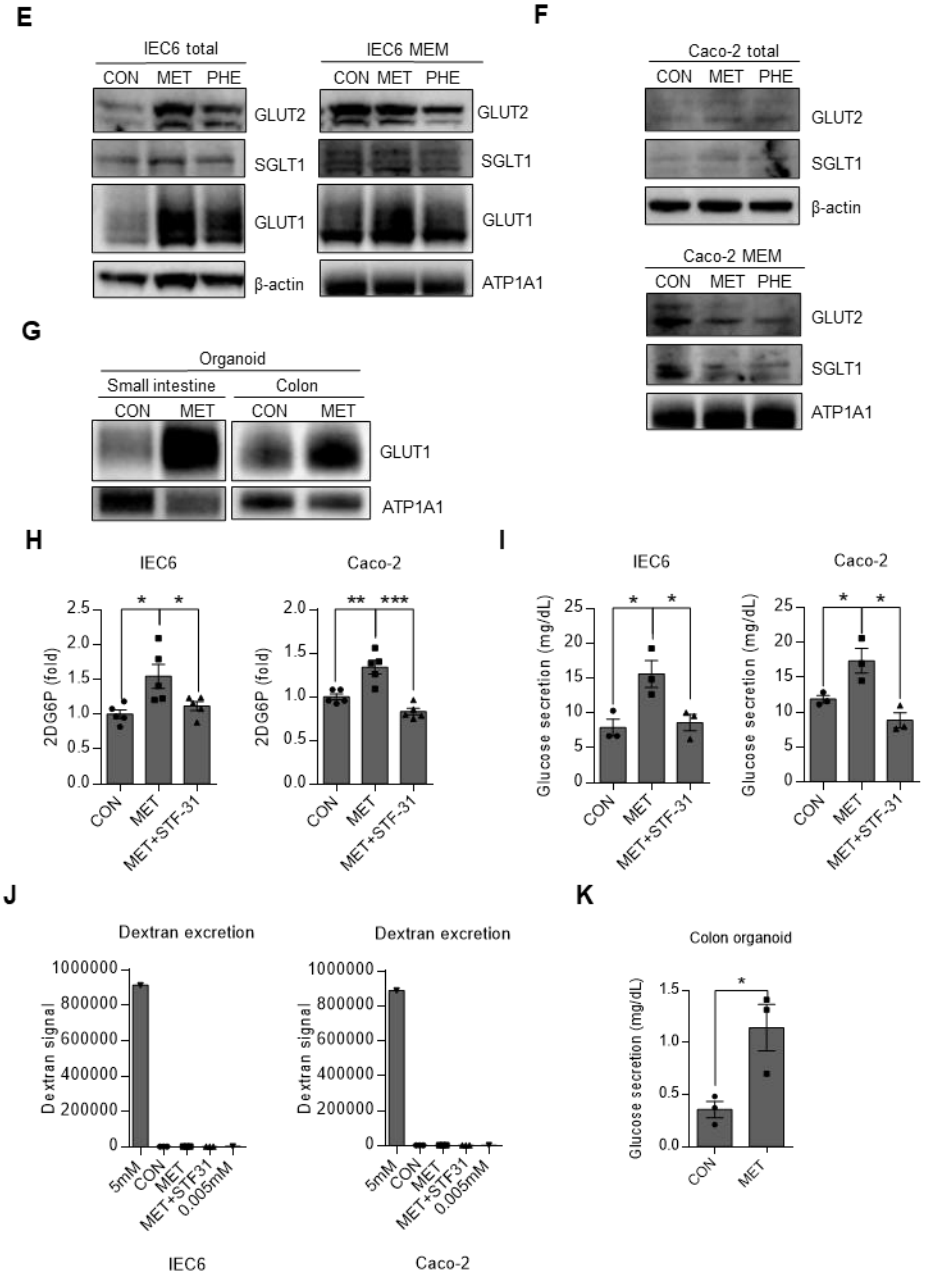

Figure 2. Metformin induces a glucotonic effect in small intestine and colon cell lines by upregulating GLUT1 expression and enhancing glycolysis. GLUT1 and glycolysis are increased in metformin-treated(5mM) small intestine and colon cell line (**A**)

qRT-PCR result of Representative gene list and corresponding fold changes in expression from metformin-treated rat small intestine (IEC6) and human colon (Caco-2) cell lines. (**B**) qRT-PCR result of glucose transporter 1(GLUT1) and glycolysis (HK2) mRNA in biguanides (metformin, phenformin)-treated IEC6 and Caco-2. (**C-F**), IEC6 and Caco-2 cell lines were incubated in the absence or presence of biguanides for 16 hours, after 8 hours starvation in serum free media, and later collected for immunoblotting of GLUT1. (**C**) Total proteins showing that GLUT1 increases in IEC6 and Caco-2 cell lines after biguanides-treated. Expression levels were normalized to that of β-actin. (**D**) Membrane proteins showing that GLUT1 increases in IEC6 and Caco-2 cell lines plasma membrane after two representative biguanides-treated. Expression levels were normalized to that of Na^+/K^+-ATPase (ATP1A1). (**E**) Total and membrane protein of IEC6. (**F**) Total and membrane protein of Caco-2. (**G**) Immunoblots of plasma membrane lysates of organoids. ATP1A1 served as a loading control of membrane protein. (**H**) Glucose uptake increased after metformin-treated in small intestine and colon cell lines. Glucose uptake detected of 2-deoxyglucose-6-phosphate (2DG6P) 2DG6P was normalized with MTS. Glucose uptake abolished after GLUT1 specific inhibitor (STF-31) treated in metformin-treated IEC6 and Caco-2 cell lines. (**I**) Glucose excretion increased after metformin-treated in IEC6 and Caco-2 cell lines. Glucose excretion abolished after GLUT1 specific inhibitor (STF-31) treated in metformin-treated IEC6 and Caco-2 cell lines. (**J**) Dextran signal in down well of transwell compared to standard signal 5mM (input amount of upper wells) and 0.005mM. Dextran signal of media used in Fig. 2I. (**K**) Glucose excretion increased in metformin treated monolayer colon organoid. Quantifying based on the protein amount in each well.All data are presented as the mean ± SEM. All data with statistical indicators were analyzed using two-tailed Student's t-tests; *$P < 0.05$, **$P < 0.01$, ***$P < 0.001$.

3.3. Metformin enhances GLUT1 expression via suppressing TXNIP

To examine the upregulation of GLUT1 associated with metformin treatment, we compared gene expression in selected regions of the ileum showing higher FDG uptake in the metformin-treated group, with basal levels observed in the vehicle-treated group using RNA sequencing. Analysis of RNA sequencing data from ileum samples revealed significant modulation of pathways by metformin (Figure 3A-3C). A strong correlation was observed between these pathways and the top Gene Ontology (GO) pathways, with the highest enrichment scores for GLUT1 (Figure 3B). This observation suggests a robust association between the pathways altered by metformin and the metformin-induced increase in GLUT1 expression. To elucidate the mechanism underlying metformin-induced increase in GLUT1 expression we comparatively analyzed the proteins implicated in RNA sequencing data that impact GLUT1 membrane trafficking[24,41-43]. Among them, GO pathways associated with TXNIP, which decreases GLUT1 expression and membrane trafficking[24,43], exhibited high similarity with GLUT1 (Figure 3E). Furthermore, a significant decrease in TXNIP levels was observed following metformin treatment. However, other known regulators of GLUT1 membrane trafficking, such as Sorting Nexin 27 (SNX27)[42] and TBC1 domain family member 5 (TBC1D5)[41], exhibited insignificant changes after metformin treatment (Figure 3F and Figure 3G). Further analysis confirmed that the expression of glucose transporters other than GLUT1 was either insignificantly altered or decreased (Figure 3F and Figure 3G). In addition to increasing GLUT1 expression, metformin treatment led to a consistent reduction in GLUT2, GLUT5, and SGLT1 expression across intestinal tissues (Figure 3F), suggesting suppressed glucose and fructose absorption from the lumen to blood, potentially contributing to systemic glucose lowering[44]. To validate the metformin-induced changes in TXNIP mRNA expression, we treated IEC6 and Caco-2 cells with biguanides. Both cell lines exhibited a notable decrease in TXNIP expression after treatment with biguanides, including metformin, phenformin, and buformin (Figure 3H). However, SNX27 and TBC1D5 mRNA levels did not show a consistently significant pattern across the biguanide groups, in line with RNA sequencing

data (Figure 3I and Figure 3J). Next, we assessed the protein levels of TXNIP in IEC6 and Caco-2 cells. Treatment with metformin and other biguanides led to a dose-dependent decrease in TXNIP expression (Figure 3K). The expression of TXNIP was significantly decreased in both cell lines and in both mouse intestinal and colorectal organoid membrane proteins, whereas GLUT1 levels were significantly increased by metformin administration (Figure 3L and Figure 3M). These results indicate that metformin increased GLUT1 membrane localization by decreasing TXNIP expression.

Previous research has demonstrated that metformin inhibits mitochondrial complex 1 of the electron transport chain[4,45] and activates AMPK [5,6]; therefore, we sought to determine which of these mechanisms was associated with GLUT1 expression upregulation. IEC6 cells were subjected to treatment with metformin alone, post-metformin treatment with the AMPK inhibitor (compound C), or rotenone, a known complex 1 inhibitor[46,47], alone. Cells co-treated with metformin and compound C exhibited upregulated GLUT1 expression and downregulated TXNIP expression compared to results in control (Figure 3N). To further confirm whether AMPK inhibition influences metformin-induced GLUT1 upregulation, AMPK was knocked down using siRNA as an alternative approach to pharmacological inhibition. Consistent with our previous findings, AMPK knockdown did not abolish the metformin-induced upregulation of GLUT1 expression (Figure 3O). These data collectively indicate that AMPK activation is not required for metformin-induced GLUT1 increase and TXNIP reduction. Rather, the metformin-mediated decrease in TXNIP expression appears to primarily involve a pathway independent of AMPK activation. Cells treated with rotenone exhibited upregulated GLUT1 expression and downregulated TXNIP expression like those treated with metformin (Figure 3P). Additionally, to determine whether direct TXNIP suppression could mimic the effects of metformin, IEC6 cells were transfected with TXNIP-specific siRNA (siTXNIP). As expected, siTXNIP transfection significantly decreased TXNIP expression in IEC6 cells (Figure 3Q). These findings further support the notion that TXNIP plays a critical role in mediating metformin-induced GLUT1 upregulation.

Next, we explored the mechanism underlying metformin-induced TXNIP suppression by examining mitochondrial complex I inhibition and associated antioxidant remodeling. Because TXNIP expression decreases under conditions of reduced ROS[48], we hypothesized that metformin lowers intracellular ROS by enhancing antioxidant defenses and NADPH availability. Analysis of our RNA-seq data revealed a trend toward increased expression of key antioxidant genes, including GSTA1–4 and TXNRD1, following metformin treatment (Figure 3R). These enzymes are involved in detoxification processes and thioredoxin recycling, respectively, suggesting transcriptional activation of antioxidant systems. Notably, expression of malic enzyme 1 (ME1), a cytosolic enzyme generated from malate, was elevated (Figure 3R). Since NADPH is crucial for antioxidant pathways, such as glutathione and thioredoxin, ME1 upregulation suggests enhanced cellular capacity for ROS. Consistently, increased ME1 and TXNRD1 expression was confirmed in intestinal tissues from metformin-treated mice, validating antioxidant remodeling in vivo (Figure 3S).

Moreover, genes associated with NADH consumption or conversion to NADPH, including LDHA, BADH (ALDH9A1), NNT, and NADK2, were also upregulated by metformin treatment in intestinal tissues (Figure 3S). Considering that metformin-induced mitochondrial complex I inhibition impairs NADH oxidation and elevates NADH levels, these transcriptional changes likely represent a compensatory adaptation to restore redox homeostasis by enhancing NADPH generation. Similar results were observed in IEC6 and Caco-2 cells treated with metformin, demonstrating consistent ME1 and TXNRD1 upregulation (Figure 3T), supporting that metformin induces similar antioxidant remodeling in vitro. Taken together, these results support a model in which metformin suppresses TXNIP expression not through AMPK activation, but via mitochondrial complex I inhibition, leading to increased NADPH production, enhanced antioxidant gene expression, and ROS reduction.

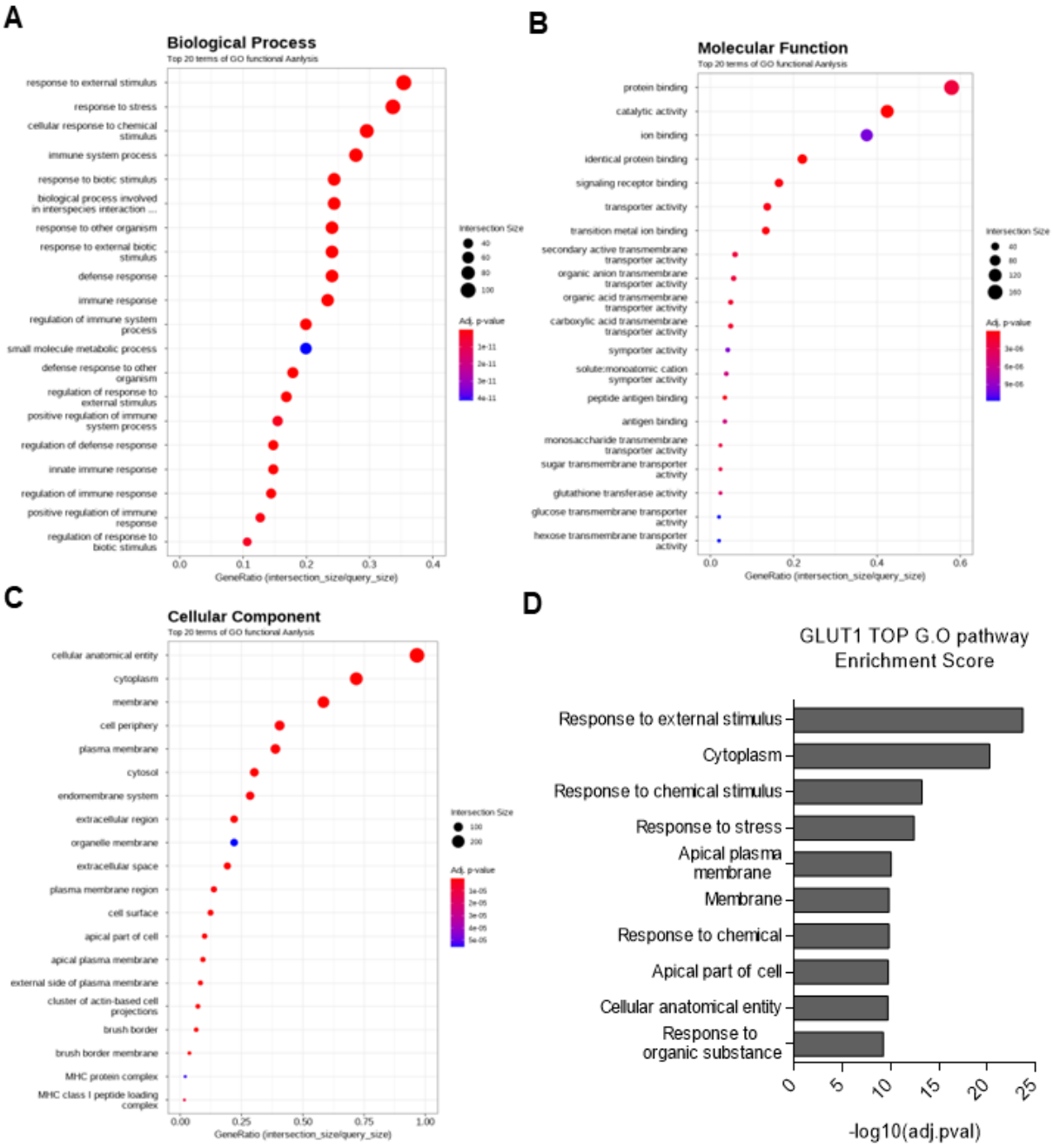

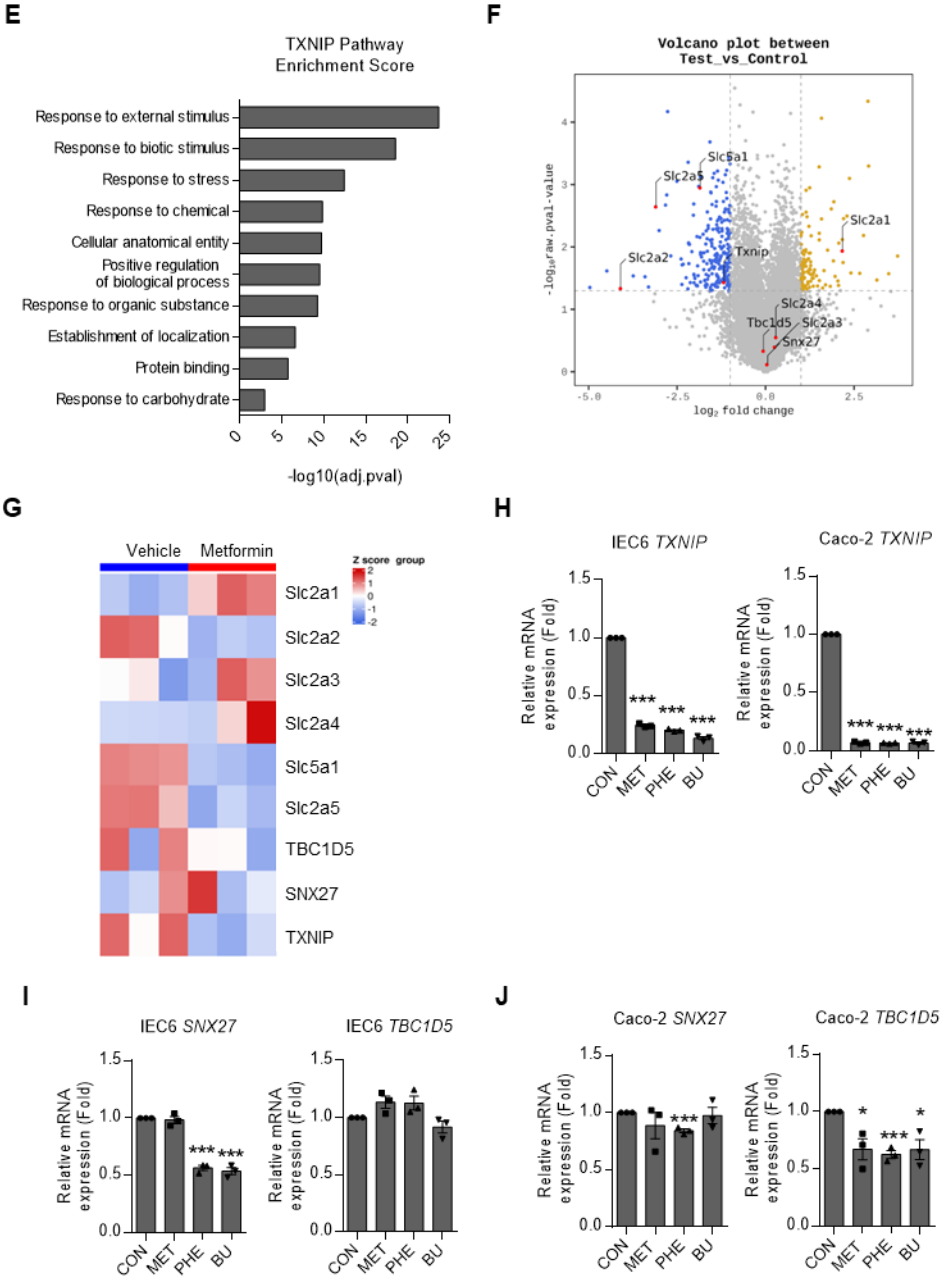

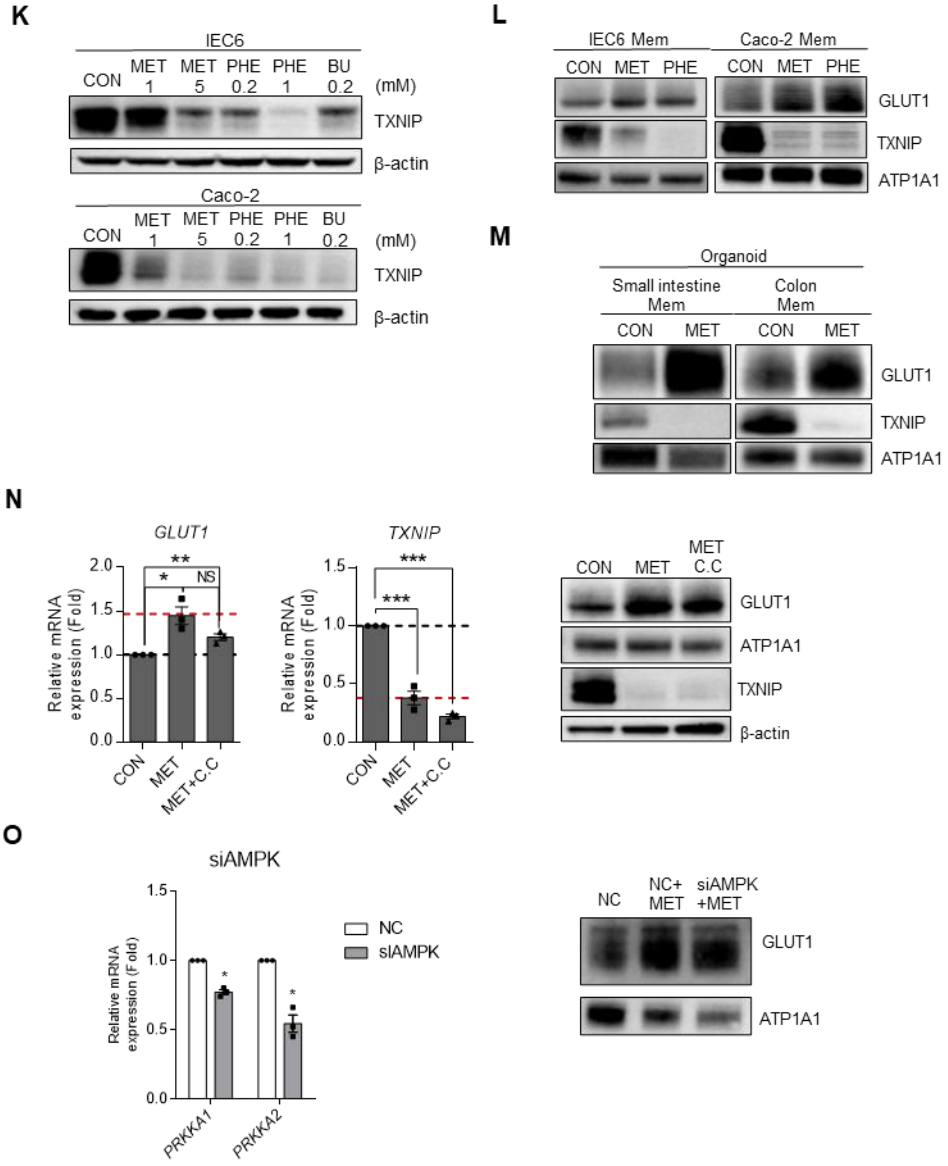

P

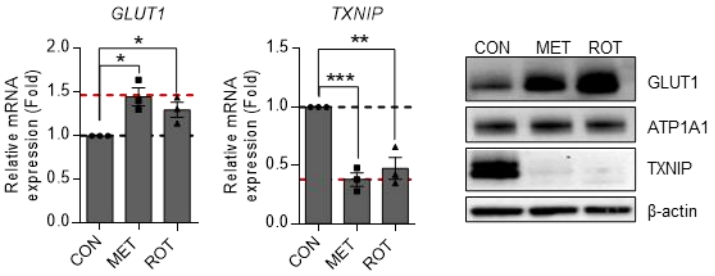

Q

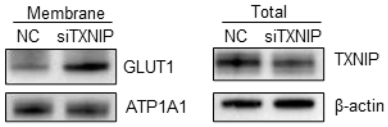

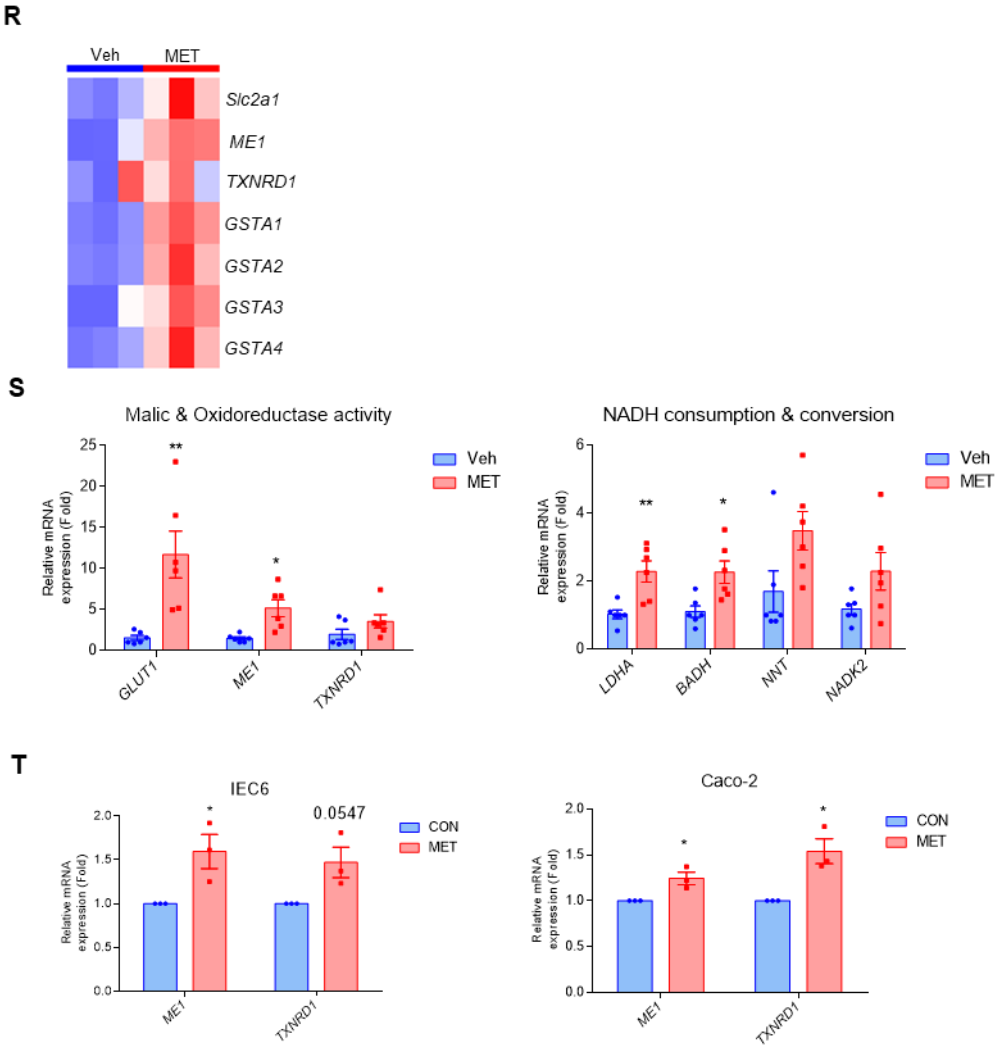

Figure 3. Metformin increases GLUT1 expression and its membrane localization in small intestine and colon cell lines by regulating TXNIP levels. Metformin increases GLUT1 membrane localization in a small intestine and colon cell line by regulating thioredoxin interacting protein (TXNIP). (**A-C**) TOP 20 terms of GO functional Analysis of (**A**) Biological Process (**B**) Molecular Function (**C**) Cellular Component after metformin gavaged mice ileum. (**D**) GLUT1 TOP G.O pathway enrichment score. (**E**) several TXNIP

pathway enrichment score. (**F**) Volcano plot that result of RNA sequencing analysis was conducted comparing the transcriptomes of mouse ileum samples from the control group to those treated with metformin. Left side of volcano plot is raw.pval<0.05 and fold change<=2, right side of volcano plot is raw.pval<0.05 and fold change>=2. (**G**) Heatmap of various glucose transporters and protein related to GLUT1 membrane localization. (**H**) qRT-PCR result of TXNIP mRNA with treated biguanides to IEC6 and Caco-2. (**I-J**) qRT-PCR result of TXNIP, SNX27 and TNC1D5 mRNA with treated biguanides to (**I**) IEC6 and (**J**) Caco-2. (**K-L**) IEC6 and Caco-2 cell lines were incubated in the absence or presence of biguanides for 16 hours, after 8 hours starvation in serum free media, and later collected for immunoblotting of TXNIP. (**K**) Total proteins showing that TXNIP decreases in IEC6 and Caco-2 cell lines after biguanides-treated. Expression levels were normalized to that of β-actin. (**L**) Membrane proteins showing that TXNIP decreases in IEC6 and Caco-2 plasma membrane after two representative biguanides-treated while GLUT1 increased. Expression levels were normalized to that of ATP1A1 (**M**) Immunoblots of plasma membrane lysates of organoids. ATP1A1 served as a loading control of membrane protein. (**N-O**) qRT-PCR and western result of GLUT1 and TXNIP after treating AMPK inhibitor and complex1 inhibitor. Black dot line indicates level of control and red dot line indicates level of metformin group. (**N**) Metformin and cotreated with metformin and AMPK inhibitor (compound c). (**O**) qRT-PCR and western result after transfect with siAMPK. **(P)** Metformin and complex1 inhibitor (Rotenon). **(Q)** Western result after transfect with siTXNIP. **(R)** Heatmap of various key antioxidant enzymes and NADPH production enzyme. **(S)** qRT-PCR result of NADPH production, antioxidant enzyme and NADH comsumption enzymes in intestinal tissues. **(T)** qRT-PCR result of NADPH production, antioxidant enzyme in IEC6 and Caco-2. All data are presented as the mean ± SEM. All data with statistical indicators were analyzed using two-tailed Student's t-tests; *P < 0.05, **P < 0.01, ***P < 0.001, NS non-significant.

3.4. TXNIP overexpression suppresses metformin-induced GLUT1 activation

We next elucidated the effect of differential TXNIP expression on GLUT1 expression in IEC6 cells overexpressing TXNIP. In these cells, metformin-induced increase in GLUT1 expression was abolished (Figure 4A). Furthermore, expression of membranous GLUT1 did not increase in these cells, even after metformin treatment (Figure 4B). Fluorescence-activated cell sorting (FACS) analysis revealed that the ratio of active GLUT1, which was significantly increased by metformin, was unchanged in cells overexpressing TXNIP (Figure 4C). Furthermore, metformin-induced glucose uptake decreased in cells overexpressing TXNIP compared with that in non-overexpressing cells (Figure 4D). These findings support the hypothesis that TXNIP overexpression inhibits metformin-induced upregulation of GLUT1 expression in enterocytes, thereby influencing glucose uptake.

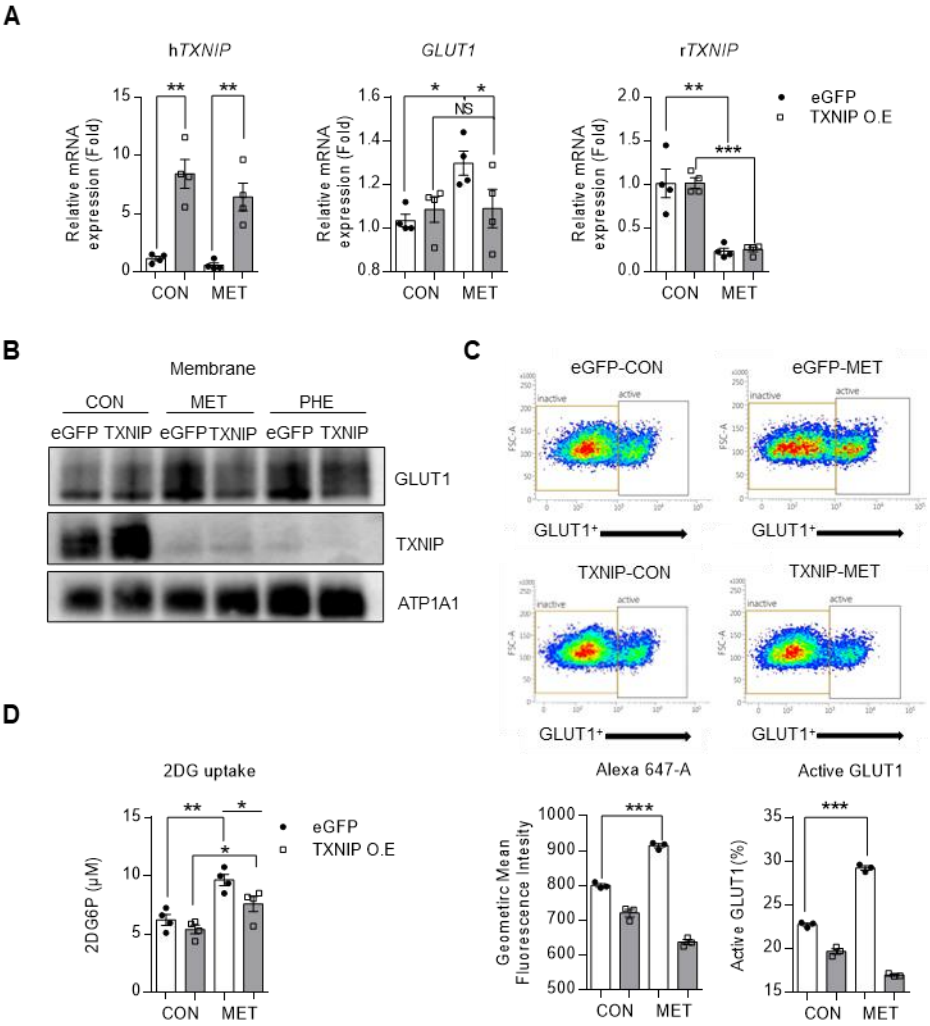

Figure 4. TXNIP overexpression inhibits metformin-induced upregulation of GLUT1 expression and glucose uptake in intestinal cell lines. Overexpression of TXNIP decrease effect of metformin that activate GLUT1 in intestinal cell line. (**A**) Expression of GLUT1, TXNIP in vehicle or metformin-treated EGFP or human TXNIP overexpressed IEC cell. (**B**) Membrane GLUT1 and TXNIP in vehicle or metformin-treated EGFP or human TXNIP overexpressed IEC6 cell. Effect of metformin-induce GLUT1 blunted in TXNIP overexpressed cell. Expression levels were normalized to that of ATP1A1. (**C**)

Representative FACS plots to analyze effect of TXNIP overexpression affect to metformin-induce GLUT1 activation are used Alexa 647. Left graphs indicate geometric mean fluorescence intensity, Right graphs indicate percentage of active GLUT1 in FACS plots. (**D**) Glucose uptake decreased compared metformin treated TXNIP overexpressed IEC6 cells with metformin treated EGFP overexpressed IEC6 cells. Glucose uptake detected of 2-deoxyglucose-6-phosphate (2DG6P). 2DG6P was normalized with MTS. All data are presented as the mean ± SEM. All data with statistical indicators were analyzed using two-tailed Student's t-tests; *P < 0.05, **P < 0.01, ***P < 0.001, NS non-significant.

3.5. Overexpression of intestinal TXNIP abolishes the glucotonic effect of metformin

TXNIP overexpression was conducted to examine the reduction in metformin efficacy and to assess the replicability of TXNIP regulation in diabetes animal models. TXNIP overexpression was induced in streptozotocin (STZ)-induced diabetic mice. The metformin dose administered to the mice in this experiment was determined to be at a therapeutically appropriate level when translated to diabetes patient treatment [49]. Notably, the blood glucose-lowering effect of metformin was abolished in the diabetic mice overexpressing TXNIP (Figure 5A). A reduction in metformin-induced enhancement of the glucotonic effect in the intestine was also abolished in TXNIP-overexpressing diabetic mice (Figure 5B and 5C). To corroborate these findings, we assessed protein expression in the ileum and colon and observed TXNIP overexpression in both tissues. TXNIP protein expression increased quantitatively in the ileum and colon tissue (Figure 5D). Conversely, no significant changes in TXNIP protein expression were noted in other organs, including the liver, kidney, heart, brain, muscle, white adipose tissue, and pancreas (Figure 5E), indicating an association between increased TXNIP levels in the distal intestine and metformin-induced blood glucose levels (Figure 5A). Subsequent examination of membranous GLUT1 expression in both tissues revealed that TXNIP overexpression led to a significant decrease of GLUT1 expression in the ileum and colon after metformin treatment, where metformin increased GLUT1 expression (Figure 5F). These results suggest an association between metformin-induced enhancement of intestinal glucose uptake and excretion, and TXNIP-mediated regulation of intestinal GLUT1 in diabetes mice.

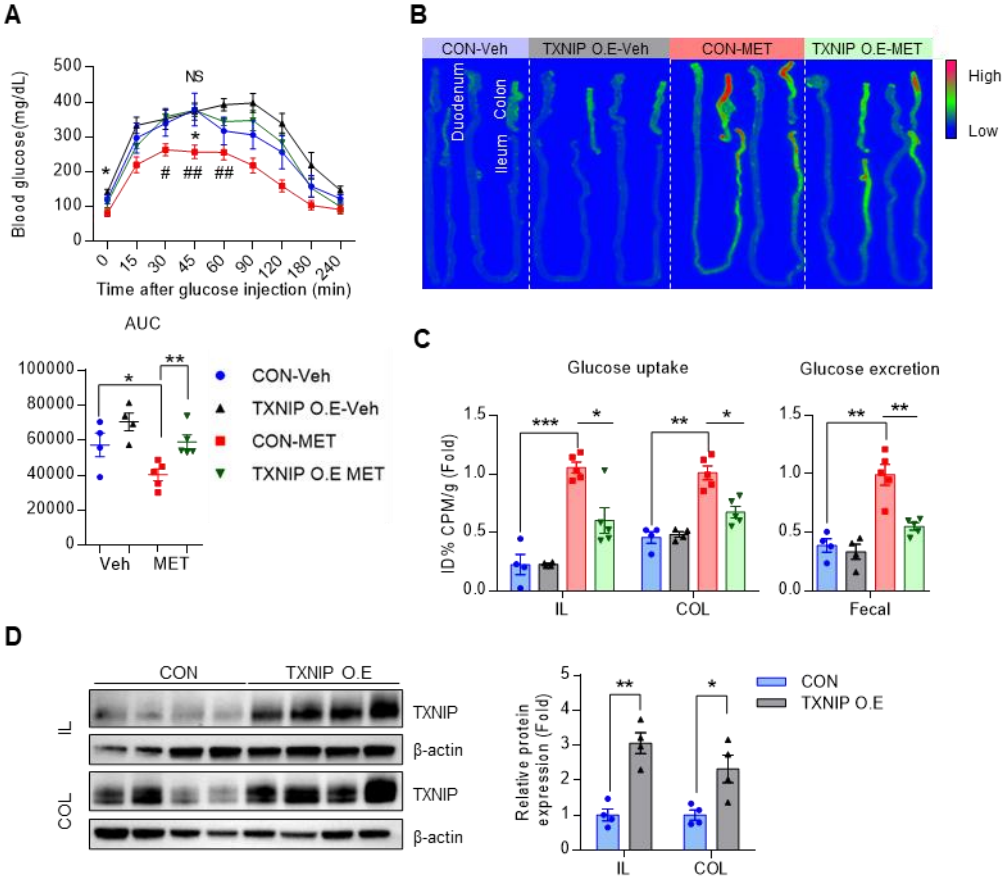

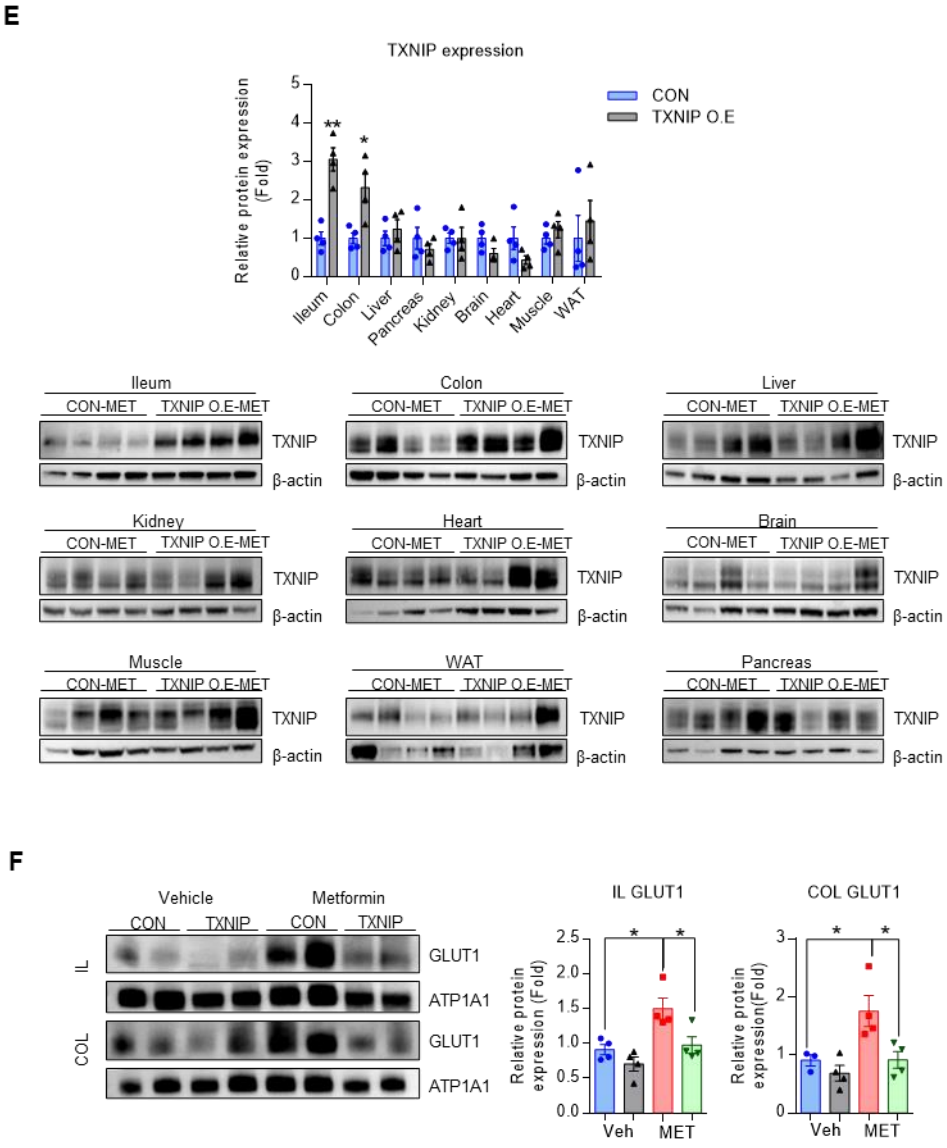

Figure 5. TXNIP overexpression in diabetic mice abolishes the blood glucose-lowering effect of metformin by reducing its enhancement of intestinal GLUT1 expression and glucotonic effect. TXNIP gene overexpression reduces metformin-induced hyperglycemia improvement in diabetics mice. (**A**) IPGTT data for vehicle and metformin treated transgenic mice. Metformin-treated non-transgenic C57BL/6 mice (n=5)

exhibited better glucose tolerance than vehicle-treated mice (n=4) and metformin-treated after TXNIP overexpressed mice (n=5, analysis of variance multiple t-test for multiple comparison correction; *P < 0.05 use to compare CON-NT and CON-MET, #P < 0.05, ##P < 0.01 use to compare CON-MET and TXMIP-MET) and corresponding AUC. (**B**) Representative images of small intestinal and colon FDG autoradiography of Metformin-treated and vehicle-treated mice after PBS lavage. Areas of higher FDG accumulation are red in colour. (**C**) Right graph shows the quantitative analysis of FDG uptake in the post-washing intestine tissue autography images. Metformin-treated limbs showed higher FDG uptake in ileum and colon compared with that in the corresponding both vehicle-treated intestine and metformin treated after TXNIP gene overexpressed. Left graph shows colon PBS washing analysis. Colon washing PBS showed larger amount of FDG excretion in the metformin-treated mice than both vehicle-treated washing PBS and metformin treated washing PBS after TXNIP gene overexpressed. (**D**) Representative images of the total protein levels of TXNIP demonstrate a significant overexpression of TXNIP in the group compared to the control group, indicating robust TXNIP upregulation in ileum and colon. Graph shows a significantly increase in TXNIP expression between control and TXNIP overexpressed groups, providing evidence of robust TXNIP upregulation. (**E**) Result of TXNIP expression in various organs compare with metformin-treated mice and metformin treated in TXNIP overexpressed transgenic mice. Graph is sum of western data quantifying based on the western data with ImageJ. (**F**) Representative images of the expression analysis of GLUT1 in membrane proteins revealed a significant increase in GLUT1 expression in the mouse intestine following metformin treatment, while a decrease was observed in mice overexpressing TXNIP, in both the ileum and colon. All data are presented as the mean ± SEM. All data with statistical indicators were analyzed using two-tailed Student's t-tests; *P < 0.05, **P < 0.01, ***P < 0.001, NS non-significant.

3.6. Intestinal GLUT1 activation is pivotal for metformin-induced glucose homeostasis

Next, we investigated the potential role of GLUT1 inhibition in mediating the glucotonic effects of metformin in vivo. For this purpose, STF-31, a specific inhibitor of GLUT1, was utilized[39,40]. Glucose uptake was significantly reduced in the distal intestine of mice co-treated with metformin and STF-31 compared to that in metformin-only-treated mice (Figure 6A and Figure 6B). Similarly, glucose excretion was also reduced in mice co-treated with metformin and STF-31 compared to that in metformin-only-treated mice (Figure 6C). The enhanced glucose homeostasis, which is associated with the intestinal glucotonic effect, was also abolished following inhibition of GLUT1 expression in metformin-treated mice (Figure 6D). However, these mice did not exhibit any significant changes in body weight in response to metformin treatment or co-treatment with metformin and STF-31 (Figure 6E). These results suggest that the metformin-induced increase in glucose homeostasis was abolished by inhibition of GLUT1 expression, particularly in the distal intestine. Furthermore, mRNA and protein expression levels were assessed in the ileum and colon, where a significant increase in the glucotonic effect was observed after metformin treatment. Both the ileum and colon exhibited significantly increased mRNA levels of GLUT1 and HK2 and decreased levels of TXNIP (Figure 6F). Conversely, no significant increase was observed in the expression of other glucose transporters (Figure 6G). Instead, reduced GLUT2 and GLUT5 expression was observed (Figure 6G). Additionally, no significant alterations were detected in the expression of gluconeogenesis-related enzymes PCK1 and G6PC (Figure 6G). The protein expression of GLUT1 was increased, whereas that of TXNIP decreased in the ileum and colon tissues treated with metformin (Figure 6H and Figure 6I). In addition, membranous protein expression of GLUT1 in both the ileum and colon increased in metformin-treated mice (Figure 6J). Subsequently, immunochemistry analysis was performed focusing on the ileum and colon, which exhibited metformin-induced glucose uptake and excretion, to elucidate the expression patterns of GLUT1 and TXNIP. In each of the four magnified figures, GLUT1

staining intensity was categorized into three levels—strong, moderate, and weak—and the distribution of these expression levels was compared across groups. IHC images revealed a clear increase in GLUT1 expression in both the ileum and colon of metformin-treated mice (Figure 6K). Quantitative analysis of staining intensity revealed a significant increase in moderate-to-strong GLUT1 expression following metformin treatment (Figure 6K). The same analysis for TXNIP showed the opposite pattern, characterized by a significant increase in weak staining intensity in both the ileum and colon of metformin-treated mice, indicating downregulation of TXNIP (Figure 6L). Notably, in vehicle-treated mice, TXNIP expression was relatively high at the villus tips of the ileum, whereas GLUT1 expression was comparatively lower in these regions (Figure 6K and Figure 6L). Additionally, immunohistochemistry analysis revealed no significant differences in GLUT1 and TXNIP protein levels in the ileum and colon of mice co-treated with metformin and STF-31 (Figure 6M). Our findings suggested that metformin increased glucose homeostasis by increasing GLUT1 expression and reducing TXNIP levels.

Finally, to confirm whether metformin also increased GLUT1 expression in the human intestine, human intestinal organoids were treated with metformin, and GLUT1 expression was compared. In human intestinal organoids, F-actin fibers are predominantly located on the apical side. GLUT1 expression was significantly increased on both the apical and basolateral sides of metformin-treated human intestinal organoids (Figure 6N). These results demonstrate that metformin suppresses TXNIP expression through mitochondrial complex 1 inhibition, leading to the upregulation of GLUT1 expression and membrane localization in the ileum and colon where it contributes to the glucotonic effect. Moreover, metformin-induced intestinal glucotonic effects play a crucial role in the regulation of glucose homeostasis.

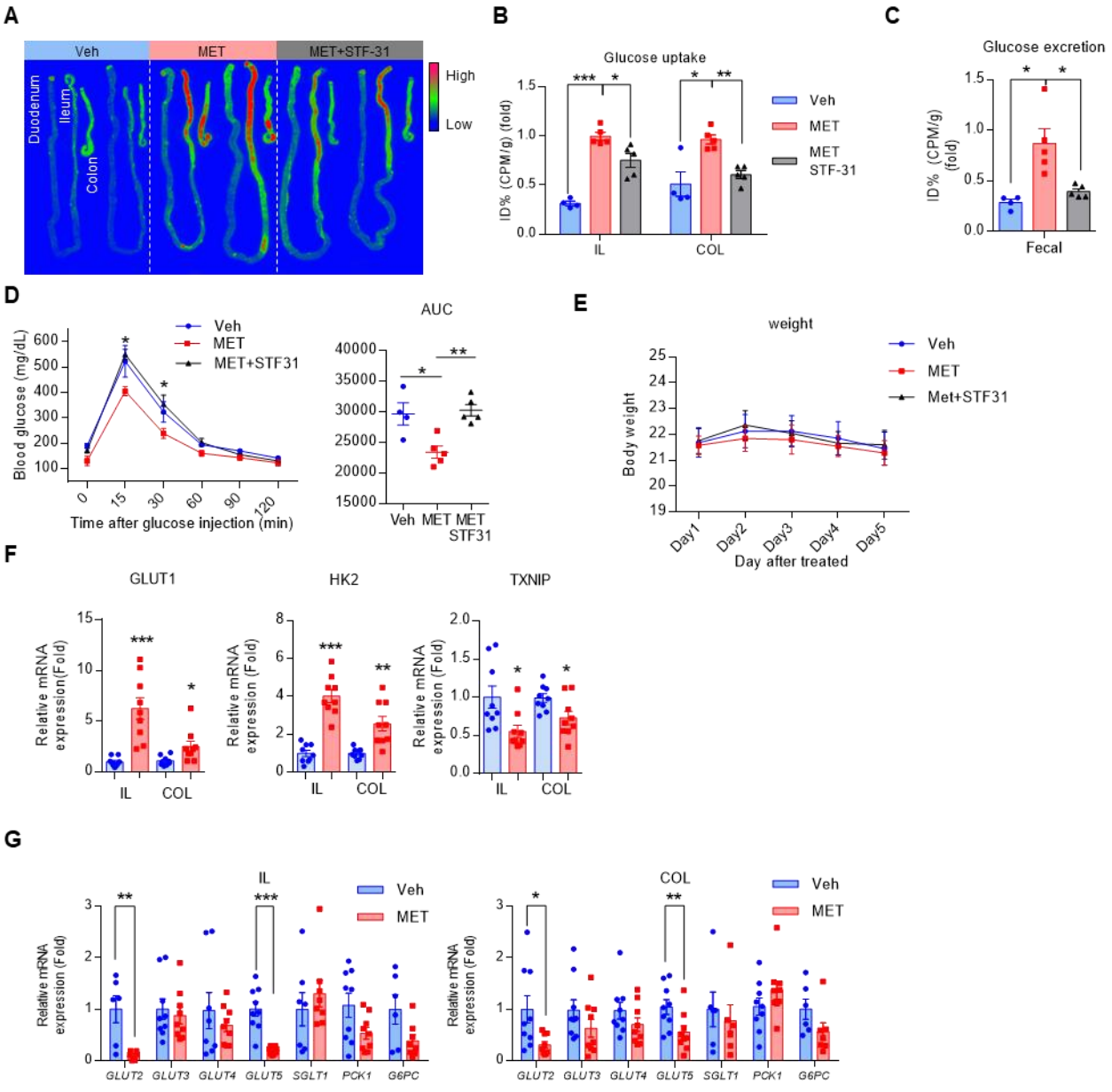

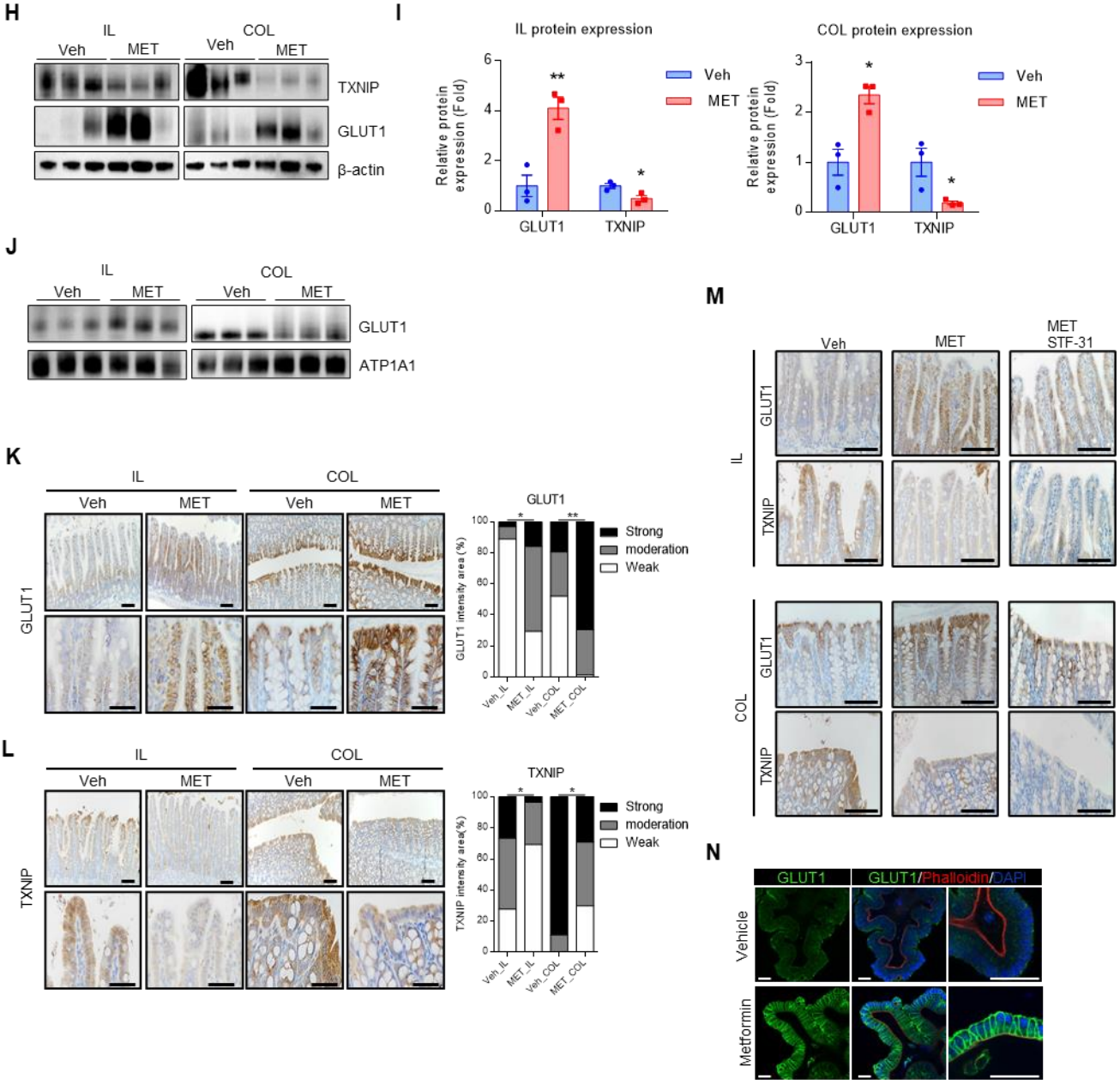

O

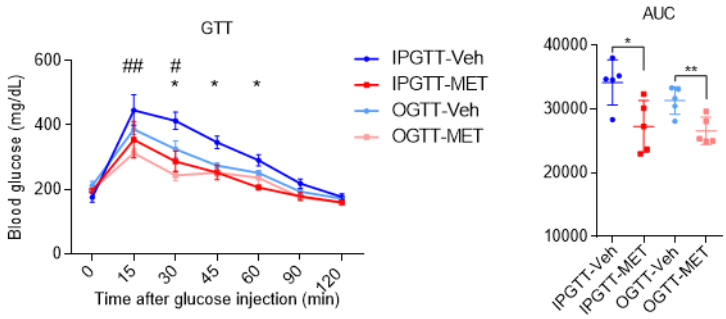

P

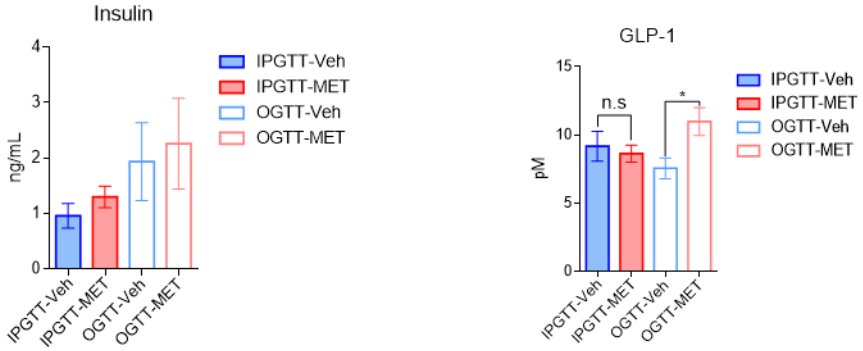

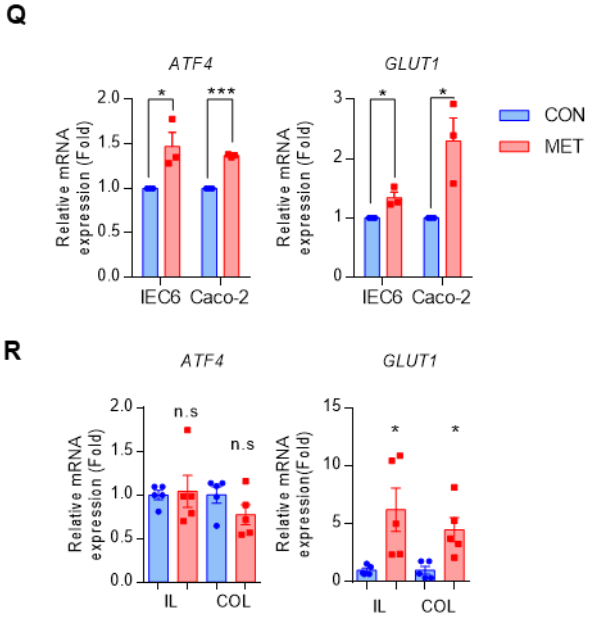

Figure 6. Inhibition of GLUT1 expression abolishes the metformin-induced increase in glucose homeostasis and glucotonic effect in the distal intestine. Blunted improvement of hyperglycemic by GLUT1 inhibitor in metformin-treat mice. (**A**) Post-washing FDG autoradiography of vehicle-treated, metformin-treated and metformin treated with STF-31 (GLUT1 specific inhibitor) I.P injection. (**B**) FDG autoradiography of the relative radiotracer amount in ileum (IL) and colon after washing. The STF-31-injected IL and colon shows significantly lower FDG uptake than the metformin-treated ileum and colon. The vehicle-treated ileum and colon were used for comparison. (**C**) Colon PBS washing analysis. STF-31 injected colon PBS washings showed lower amount of FDG excretion than the metformin-treated mice. The vehicle-treated ileum and colon were used for comparison. (**D**) Intraperitoneal glucose tolerance test (IPGTT) data for metformin with GLUT1 inhibitor (STF-31)-I.P injection, metformin-treated and vehicle-treated mice. Metformin group showed significant improvement in glucose tolerance compared with that in the vehicle group. This improvement in glucose tolerance was significantly reduced in the metformin with STF-31 injection group compared with that in the metformin group

(n=5, analysis of variance multiple t-test for multiple comparison correction) and corresponding area under the curve (AUC). (**E**) Body weight after metformin and STF-31 treatment. Mice did not exhibit any significant changes in body weight in response to metformin or co-treated metformin and STF-31 treatment. (**F**) Expression of GLUT1, HK2, TXNIP in ileum and colon from vehicle and metformin treated mice. (**G**) Expression of various glucose transporter and gluconeogenesis enzyme in ileum and colon from vehicle and metformin treated mice. (**H**) The immunoblot shows the increased GLUT1 and decreased TXNIP both ileum and colon samples from metformin-treated mice (n = 3 mice/group). Expression levels were normalized to that of β-actin. (**I**) Graph shows comparison of protein expression of Figure 6H quantify with ImageJ. (**J**) Membrane GLUT1 expression in ileum and colon from vehicle and metformin treated mice (n = 3 mice/group). Expression levels were normalized to that of ATP1A1. (**K-M**) Representative images of GLUT1 and TXNIP immunostaining of the ileum and colon from vehicle-treated and metformin-treated C57BL/6 mice. Scale bars of left images indicate 100μm and scale bars of right images indicate 50μm. (**K-L**) Statistical comparisons were performed on the percentage of strongly DAB-stained area between vehicle and metformin-treated groups. (**K**) GLUT1 (**L**) TXNIP. (**M**) Representative images of GLUT1 and TXNIP immunostaining of the ileum and colon from vehicle-treated, metformin-treated and cotreated with metformin and STF-31 C57BL/6 mice. (**N**) Representative fluorescence images of GLUT1 after vehicle and metformin treated in human intestinal organoid. Red signals represent phalloidin 4 staining, indicating F-actin fibers. Blue signals represent DAPI staining, indicating nuclei location and green signal representing GLUT1 expression. Scale bars of image indicate 50μm. (**O**) IPGTT and OGTT data for vehicle and metformin treated mice. Metformin-treated C57BL/6 mice (n = 5) exhibited improved glucose tolerance compared to vehicle-treated mice (n = 5) in both OGTT and IPGTT. No significant difference in total AUC was observed between OGTT and IPGTT. However, in OGTT, the glucose-lowering effect of metformin appeared earlier, with notable differences between groups observed at early time points (15–30 min). In contrast, IPGTT revealed

group differences at later time points (30–60 min), indicating a delayed response consistent with reduced incretin involvement (analysis of variance multiple t-test for multiple comparison correction; *P < 0.05 use to compare IPGTT-Veh and IPGTT-MET, #P < 0.05, ##P < 0.01 use to compare OGTT-Veh and OGTT-MET). (**P**) Plasma insulin and GLP-1 levels following OGTT and IPGTT in vehicle- and metformin-treated mice. At 15 minutes post-glucose administration, plasma insulin levels tended to be higher in OGTT compared to IPGTT. Additionally, GLP-1 levels showed the highest tendency in the OGTT-metformin group, suggesting that the earlier glucose-lowering effect observed with OGTT may be associated with incretin hormone responses. (**Q**) After metformin treated in IEC6 and Caco-2 cell line. (**R**) Metformin(red) treated ileum and colon compare to Vehicle(blue). All data are presented as the mean ± SEM. All data with statistical indicators were analyzed using two-tailed Student's t-tests; *P < 0.05, **P < 0.01, ***P < 0.001.

4. DISCUSSION

This study demonstrated that metformin exerts its glucose-lowering effects primarily by modulating intestinal glucose handling through increased glucose uptake and excretion in the distal intestine, specifically the ileum and colon. These effects result from enhanced expression and membrane trafficking of GLUT1, mediated via TXNIP downregulation due to mitochondrial complex I inhibition. Consistent with this mechanism, metformin treatment reduced blood glucose in both diabetic and non-diabetic mouse models, accompanied by increased GLUT1 and decreased TXNIP expression, compared to other glucose transporters. These findings were further validated in intestinal cell lines derived from rats and humans, as well as mouse and human intestinal organoids.

Metformin is known to enhance glucose homeostasis partly by increasing incretin hormone secretion, particularly GLP-1[50,51]. To explore alternative mechanisms—especially its reported effect on intestinal glucose uptake—we aimed to minimize the confounding influence of incretin signaling. We therefore compared metformin's effects via both OGTT and IPGTT, as the latter is known to elicit a weaker incretin response[52,53]. As shown in Figure 6O, metformin lowered blood glucose in both tests; however, the reduction occurred earlier in OGTT and was delayed in IPGTT, consistent with prior studies. Insulin level was higher in OGTT than in IPGTT, while GLP-1 levels remained relatively similar across groups, with only a modest increase in the OGTT-MET group (Figure 6P). Based on these findings, we selected IPGTT as our primary method to evaluate metformin's incretin-independent actions.

Previous investigations using FDG imaging have associated increased intestinal glucose uptake with improved glucose regulation following bariatric surgery and metformin treatment[26,28]. Although the AMPK and activating transcription factor 4 (ATF4) pathways have previously been implicated in GLUT1 regulation, our findings indicate that metformin-induced GLUT1 upregulation occurs independently of both. AMPK inhibition, either pharmacologically using compound C or through siRNA-mediated knockdown, did

not block the increase in GLUT1 expression following metformin treatment (Figure 3N and Figure 3O), supporting an AMPK-independent mechanism. Regarding ATF4, previous studies have reported that metformin increases its expression in vitro[26,54]. Consistent with these reports, we observed elevated ATF4 levels in intestinal cell lines following metformin treatment (Figure 6Q). However, this effect was not reproduced in vivo: in the ileum and colon of metformin-treated mice, GLUT1 expression was markedly increased, whereas ATF4 levels remained unchanged (Figure 6R, GSE271623). These findings indicate that ATF4 does not contribute to GLUT1 regulation in intestinal tissues. Instead, our data (Figure 3F, Figure 3R and Figure 3S) support a mechanism in which mitochondrial complex I inhibition promotes antioxidant gene expression and NADPH production, leading to TXNIP suppression and subsequent GLUT1 upregulation.

Among various glucose transporters, GLUT1 was uniquely and consistently upregulated by metformin, and its expression remained elevated even under AMPK inhibition (Figure 3N and Figure 3O). Similarly, treatment with rotenone or siTXNIP—targeting mitochondrial complex I or TXNIP, respectively—recapitulated the metformin-induced increase in GLUT1 (Figure 3P and Figure 3Q). These results suggest that metformin promotes GLUT1 expression through TXNIP suppression, independently of AMPK, and likely via mitochondrial complex I inhibition. Supporting this mechanism, metformin also increased the expression of antioxidant-related enzymes in intestinal tissues and cells (Figure 3R-3T), including ME1, which generates NADPH to support antioxidant activity. Genes involved in the conversion or consumption of excess NADH, which may accumulate due to complex I inhibition, were similarly upregulated (Figure 3S). These findings suggest that metformin suppresses TXNIP expression through a redox-based, AMPK-independent mechanism, thereby promoting GLUT1 upregulation. Consistent with this mechanism, inhibition of GLUT1 abolished the glucose-lowering effect of metformin in mice (Figure 6D), highlighting the critical role of GLUT1 in mediating the metabolic actions of metformin.

In addition to increased GLUT1 expression, our data consistently showed reduced expression of GLUT2 and GLUT5 following metformin treatment (Figure 2A and Figure 3G and Figure 6G). SGLT1 was also downregulated under metformin treatment (Figure 3G) GLUT2 is localized to the basolateral membrane of enterocytes and facilitates glucose transfer from the intestinal lumen into the bloodstream, thereby contributing to elevated blood glucose levels[18,44,55]. Similarly, SGLT1 is expressed on the apical membrane and mediates active glucose uptake from the lumen into enterocytes[18,44]. The downregulation of both transporters may thus contribute to reduced systemic glucose levels. Supporting this interpretation, a previous clinical study reported that individuals carrying SNPs associated with reduced GLUT2 expression exhibit greater responsiveness to metformin, further suggesting that decreased intestinal glucose absorption mediated by reduced expression of glucose transporters such as GLUT2, may play an important role in enhancing overall glucose homeostasis following metformin administration.[56]. The decrease in GLUT5, a fructose transporter, may reflect a compensatory response to increased GLUT1-mediated glucose efflux or represent an independent regulatory effect[57]. Moreover, the concurrent increase in HK2 expression, without a corresponding rise in gluconeogenic enzymes (G6PC and PCK1), suggests preferential glycolytic rather than gluconeogenic metabolism in the intestine following metformin administration. Interestingly, we observed a modest increase in PCK1 expression in Caco-2 cells and the colon, though not statistically significant in the latter, implying that gluconeogenic responses may vary between the ileum and colon.

While concerns could arise regarding potential oncogenic effects due to increased GLUT1 expression, existing evidence strongly supports metformin's anticancer properties[58-64]. Indeed, increased GLUT1 expression localized to intestinal epithelial membranes facilitates luminal glucose excretion, potentially reducing intracellular glucose accumulation and mitigating the Warburg effect, a hallmark of tumor metabolism. Thus, the enhanced GLUT1 expression induced by metformin in our model likely complements its well-established antitumor actions.

Despite its robust findings, this study has limitations. First, we did not include direct analysis of human intestinal tissues from metformin-treated individuals; however, consistent results obtained from human intestinal cell lines and organoids strengthen the translational relevance of our findings. Additionally, while we effectively achieved intestine-specific TXNIP overexpression via plasmid-mediated delivery, long-term effects were not evaluated. Nevertheless, previous long-term studies of TXNIP overexpression indicate persistent glucose dysregulation without affecting body weight[65], supporting the physiological significance of TXNIP suppression for glucose homeostasis. Although we employed a mild STZ-induced diabetic mouse model that mimics certain aspects of type 2 diabetes, the inclusion of additional insulin-resistant or diet-induced models in future studies could enhance generalizability. Nonetheless, despite these limitations, our study offers significant insights into the direct impact of metformin on intestinal glucose metabolism highlighting the role of TXNIP downregulation and GLUT1 upregulation as key mechanism of its glucose-lowering effect. The consistent findings across various species and models strengthen the translational potential of this mechanism, providing a foundation for future research aimed at refining therapeutic strategies and highlighting the potential of modulating GLUT1 expression in various disease contexts.

5. CONCLUSION

In conclusion, our study uncovers a novel intestinal mechanism underlying metformin's glucose-lowering action. By inhibiting mitochondrial complex I and suppressing TXNIP, metformin promotes GLUT1 expression and trafficking to intestinal epithelial membranes, increasing glucose excretion and uptake in the distal intestine. These findings highlight the therapeutic potential of targeting the intestinal TXNIP–GLUT1 axis and offer novel avenues for improving glucose homeostasis beyond conventional antidiabetic strategies.

References

1. Foretz M, Guigas B, Bertrand L, Pollak M, Viollet B. Metformin: from mechanisms of action to therapies. Cell Metab 2014;20:953-66.
2. Bailey CJ. Metformin: historical overview. Diabetologia 2017;60:1566-76.
3. Foretz M, Guigas B, Viollet B. Metformin: update on mechanisms of action and repurposing potential. Nat Rev Endocrinol 2023;19:460-76.
4. Owen MR, Doran E, Halestrap AP. Evidence that metformin exerts its anti-diabetic effects through inhibition of complex 1 of the mitochondrial respiratory chain. Biochem J 2000;348 Pt 3:607-14.
5. Zhou G, Myers R, Li Y, Chen Y, Shen X, Fenyk-Melody J, et al. Role of AMP-activated protein kinase in mechanism of metformin action. J Clin Invest 2001;108:1167-74.
6. Musi N, Hirshman MF, Nygren J, Svanfeldt M, Bavenholm P, Rooyackers O, et al. Metformin increases AMP-activated protein kinase activity in skeletal muscle of subjects with type 2 diabetes. Diabetes 2002;51:2074-81.
7. Shaw RJ, Lamia KA, Vasquez D, Koo SH, Bardeesy N, Depinho RA, et al. The kinase LKB1 mediates glucose homeostasis in liver and therapeutic effects of metformin. Science 2005;310:1642-6.
8. Shin NR, Lee JC, Lee HY, Kim MS, Whon TW, Lee MS, et al. An increase in the Akkermansia spp. population induced by metformin treatment improves glucose homeostasis in diet-induced obese mice. Gut 2014;63:727-35.
9. Horakova O, Kroupova P, Bardova K, Buresova J, Janovska P, Kopecky J, et al. Metformin acutely lowers blood glucose levels by inhibition of intestinal glucose transport. Sci Rep 2019;9:6156.
10. Song Y, Koehler JA, Baggio LL, Powers AC, Sandoval DA, Drucker DJ. Gut-Proglucagon-Derived Peptides Are Essential for Regulating Glucose Homeostasis in Mice. Cell Metab 2019;30:976-86.e3.
11. Maselli DB, Camilleri M. Effects of GLP-1 and Its Analogs on Gastric Physiology in Diabetes Mellitus and Obesity. Adv Exp Med Biol 2021;1307:171-92.
12. Portincasa P, Bonfrate L, Vacca M, De Angelis M, Farella I, Lanza E, et al. Gut Microbiota and Short Chain Fatty Acids: Implications in Glucose Homeostasis. Int J Mol Sci 2022;23.
13. Wang P, Sun H, Maitiabula G, Zhang L, Yang J, Zhang Y, et al. Total parenteral nutrition impairs glucose metabolism by modifying the gut microbiome. Nat Metab 2023;5:331-48.
14. Shin JH, Bozadjieva-Kramer N, Shao Y, Lyons-Abbott S, Rupp AC, Sandoval DA, et al. The gut peptide Reg3g links the small intestine microbiome to the regulation of energy balance, glucose levels, and gut function. Cell Metab 2022;34:1765-78.e6.
15. Zake DM, Kurlovics J, Zaharenko L, Komasilovs V, Klovins J, Stalidzans E. Physiologically based metformin pharmacokinetics model of mice and scale-up to humans for the estimation of concentrations in various tissues. PLoS One 2021;16:e0249594.
16. Mueckler M, Thorens B. The SLC2 (GLUT) family of membrane transporters. Mol Aspects Med 2013;34:121-38.
17. Deng D, Xu C, Sun P, Wu J, Yan C, Hu M, et al. Crystal structure of the human glucose transporter GLUT1. Nature 2014;510:121-5.
18. Koepsell H. Glucose transporters in the small intestine in health and disease. Pflugers Arch 2020;472:1207-48.

19. Choi EH, Park SJ. TXNIP: A key protein in the cellular stress response pathway and a potential therapeutic target. Exp Mol Med 2023;55:1348-56.
20. Chen J, Saxena G, Mungrue IN, Lusis AJ, Shalev A. Thioredoxin-interacting protein: a critical link between glucose toxicity and beta-cell apoptosis. Diabetes 2008;57:938-44.
21. Parikh H, Carlsson E, Chutkow WA, Johansson LE, Storgaard H, Poulsen P, et al. TXNIP regulates peripheral glucose metabolism in humans. PLoS Med 2007;4:e158.
22. Minn AH, Hafele C, Shalev A. Thioredoxin-interacting protein is stimulated by glucose through a carbohydrate response element and induces beta-cell apoptosis. Endocrinology 2005;146:2397-405.
23. Dykstra H, LaRose C, Fisk C, Waldhart A, Meng X, Zhao G, et al. TXNIP interaction with GLUT1 depends on PI(4,5)P(2). Biochim Biophys Acta Biomembr 2021;1863:183757.
24. Qualls-Histed SJ, Nielsen CP, MacGurn JA. Lysosomal trafficking of the glucose transporter GLUT1 requires sequential regulation by TXNIP and ubiquitin. iScience 2023;26:106150.
25. Morita Y, Nogami M, Sakaguchi K, Okada Y, Hirota Y, Sugawara K, et al. Enhanced Release of Glucose Into the Intraluminal Space of the Intestine Associated With Metformin Treatment as Revealed by [(18)F]Fluorodeoxyglucose PET-MRI. Diabetes Care 2020;43:1796-802.
26. Tobar N, Rocha GZ, Santos A, Guadagnini D, Assalin HB, Camargo JA, et al. Metformin acts in the gut and induces gut-liver crosstalk. Proc Natl Acad Sci U S A 2023;120:e2211933120.
27. Ku CR, Lee N, Hong JW, Kwon IG, Hyung WJ, Noh SH, et al. Intestinal Glycolysis Visualized by FDG PET/CT Correlates With Glucose Decrement After Gastrectomy. Diabetes 2017;66:385-91.
28. Kwon IG, Kang CW, Park JP, Oh JH, Wang EK, Kim TY, et al. Serum glucose excretion after Roux-en-Y gastric bypass: a potential target for diabetes treatment. Gut 2021;70:1847-56.
29. Oh JH, Kang CW, Wang EK, Nam JH, Lee S, Park KH, et al. Altered Glucose Metabolism and Glucose Transporters in Systemic Organs After Bariatric Surgery. Front Endocrinol (Lausanne) 2022;13:937394.
30. Kim D, Langmead B, Salzberg SL. HISAT: a fast spliced aligner with low memory requirements. Nat Methods 2015;12:357-60.
31. Pertea M, Pertea GM, Antonescu CM, Chang TC, Mendell JT, Salzberg SL. StringTie enables improved reconstruction of a transcriptome from RNA-seq reads. Nat Biotechnol 2015;33:290-5.
32. Pertea M, Kim D, Pertea GM, Leek JT, Salzberg SL. Transcript-level expression analysis of RNA-seq experiments with HISAT, StringTie and Ballgown. Nat Protoc 2016;11:1650-67.
33. Raudvere U, Kolberg L, Kuzmin I, Arak T, Adler P, Peterson H, et al. g:Profiler: a web server for functional enrichment analysis and conversions of gene lists (2019 update). Nucleic Acids Res 2019;47:W191-w8.
34. Baud G, Daoudi M, Hubert T, Raverdy V, Pigeyre M, Hervieux E, et al. Bile Diversion in Roux-en-Y Gastric Bypass Modulates Sodium-Dependent Glucose Intestinal Uptake. Cell Metab 2016;23:547-53.
35. Zubiaga L, Briand O, Auger F, Touche V, Hubert T, Thevenet J, et al. Oral metformin transiently lowers post-prandial glucose response by reducing the apical expression of sodium-glucose co-transporter 1 in enterocytes. iScience 2023;26:106057.

36. Ke Z, Lu Z, Li Q, Tong W. Intestinal glucose excretion: A potential mechanism for glycemic control. Metabolism 2024;152:155743.
37. Bao C, Zhu S, Song K, He C. HK2: a potential regulator of osteoarthritis via glycolytic and non-glycolytic pathways. Cell Commun Signal 2022;20:132.
38. Lenzen S, Lortz S, Tiedge M. Effect of metformin on SGLT1, GLUT2, and GLUT5 hexose transporter gene expression in small intestine from rats. Biochem Pharmacol 1996;51:893-6.
39. Chan DA, Sutphin PD, Nguyen P, Turcotte S, Lai EW, Banh A, et al. Targeting GLUT1 and the Warburg effect in renal cell carcinoma by chemical synthetic lethality. Sci Transl Med 2011;3:94ra70.
40. Boheler KR, Bhattacharya S, Kropp EM, Chuppa S, Riordon DR, Bausch-Fluck D, et al. A human pluripotent stem cell surface N-glycoproteome resource reveals markers, extracellular epitopes, and drug targets. Stem Cell Reports 2014;3:185-203.
41. Roy S, Leidal AM, Ye J, Ronen SM, Debnath J. Autophagy-Dependent Shuttling of TBC1D5 Controls Plasma Membrane Translocation of GLUT1 and Glucose Uptake. Mol Cell 2017;67:84-95.e5.
42. Shinde SR, Maddika S. PTEN Regulates Glucose Transporter Recycling by Impairing SNX27 Retromer Assembly. Cell Rep 2017;21:1655-66.
43. Sullivan WJ, Mullen PJ, Schmid EW, Flores A, Momcilovic M, Sharpley MS, et al. Extracellular Matrix Remodeling Regulates Glucose Metabolism through TXNIP Destabilization. Cell 2018;175:117-32.e21.
44. Lee HJ, Cha JY. Recent insights into the role of ChREBP in intestinal fructose absorption and metabolism. BMB Rep 2018;51:429-36.
45. Vial G, Detaille D, Guigas B. Role of Mitochondria in the Mechanism(s) of Action of Metformin. Front Endocrinol (Lausanne) 2019;10:294.
46. Gui DY, Sullivan LB, Luengo A, Hosios AM, Bush LN, Gitego N, et al. Environment Dictates Dependence on Mitochondrial Complex I for NAD+ and Aspartate Production and Determines Cancer Cell Sensitivity to Metformin. Cell Metab 2016;24:716-27.
47. Yang M, Darwish T, Larraufie P, Rimmington D, Cimino I, Goldspink DA, et al. Inhibition of mitochondrial function by metformin increases glucose uptake, glycolysis and GDF-15 release from intestinal cells. Sci Rep 2021;11:2529.
48. Liu Z, Cheng P, Feng T, Xie Z, Yang M, Chen Z, et al. Nrf2/HO-1 blocks TXNIP/NLRP3 interaction via elimination of ROS in oxygen-glucose deprivation-induced neuronal necroptosis. Brain Res 2023;1817:148482.
49. Reagan-Shaw S, Nihal M, Ahmad N. Dose translation from animal to human studies revisited. Faseb j 2008;22:659-61.
50. Bahne E, Sun EWL, Young RL, Hansen M, Sonne DP, Hansen JS, et al. Metformin-induced glucagon-like peptide-1 secretion contributes to the actions of metformin in type 2 diabetes. JCI Insight 2018;3.
51. Cravalho CKL, Meyers AG, Mabundo LS, Courville A, Yang S, Cai H, et al. Metformin improves blood glucose by increasing incretins independent of changes in gluconeogenesis in youth with type 2 diabetes. Diabetologia 2020;63:2194-204.
52. Andrikopoulos S, Blair AR, Deluca N, Fam BC, Proietto J. Evaluating the glucose tolerance test in mice. Am J Physiol Endocrinol Metab 2008;295:E1323-32.
53. Small L, Ehrlich A, Iversen J, Ashcroft SP, Trošt K, Moritz T, et al. Comparative analysis of oral and intraperitoneal glucose tolerance tests in mice. Mol Metab 2022;57:101440.

54. Coll AP, Chen M, Taskar P, Rimmington D, Patel S, Tadross JA, et al. GDF15 mediates the effects of metformin on body weight and energy balance. Nature 2020;578:444-8.
55. Sun B, Chen H, Xue J, Li P, Fu X. The role of GLUT2 in glucose metabolism in multiple organs and tissues. Mol Biol Rep 2023;50:6963-74.
56. Zhou K, Yee SW, Seiser EL, van Leeuwen N, Tavendale R, Bennett AJ, et al. Variation in the glucose transporter gene SLC2A2 is associated with glycemic response to metformin. Nat Genet 2016;48:1055-9.
57. Douard V, Ferraris RP. Regulation of the fructose transporter GLUT5 in health and disease. Am J Physiol Endocrinol Metab 2008;295:E227-37.
58. Vancura A, Bu P, Bhagwat M, Zeng J, Vancurova I. Metformin as an Anticancer Agent. Trends Pharmacol Sci 2018;39:867-78.
59. Zhao B, Luo J, Yu T, Zhou L, Lv H, Shang P. Anticancer mechanisms of metformin: A review of the current evidence. Life Sci 2020;254:117717.
60. Dutta S, Shah RB, Singhal S, Dutta SB, Bansal S, Sinha S, et al. Metformin: A Review of Potential Mechanism and Therapeutic Utility Beyond Diabetes. Drug Des Devel Ther 2023;17:1907-32.
61. Saraei P, Asadi I, Kakar MA, Moradi-Kor N. The beneficial effects of metformin on cancer prevention and therapy: a comprehensive review of recent advances. Cancer Manag Res 2019;11:3295-313.
62. Hua Y, Zheng Y, Yao Y, Jia R, Ge S, Zhuang A. Metformin and cancer hallmarks: shedding new lights on therapeutic repurposing. J Transl Med 2023;21:403.
63. Zhu L, Yang K, Ren Z, Yin D, Zhou Y. Metformin as anticancer agent and adjuvant in cancer combination therapy: Current progress and future prospect. Transl Oncol 2024;44:101945.
64. Higurashi T, Nakajima A. Metformin and Colorectal Cancer. Front Endocrinol (Lausanne) 2018;9:622.
65. Schneider MR, Zettler S, Rathkolb B, Dahlhoff M. TXNIP overexpression in mice enhances streptozotocin-induced diabetes severity. Mol Cell Endocrinol 2023;565:111885.

Abstract in Korean

새로운 메트포르민의 혈당 항상성 개선 기전: TXNIP−GLUT1 축 조절을 통한 장 내 글루코토닉 효과 증진

메트포르민은 제2형 당뇨병 관리를 위한 대표적인 약물로서 다양한 약리학적 효과를 나타내지만, 장 내 포도당 수송체 조절 기전과 그에 따른 포도당 항상성 유지와의 연관성은 아직 완전히 밝혀지지 않았다. 본 연구에서는 메트포르민이 유도하는 대사 변화와 장 내 포도당 대사 변화가 전신 포도당 항상성 개선에 미치는 영향을 조사하였다. 연구 결과, 메트포르민은 주로 회장과 대장에서 포도당 흡수 및 배출을 증가시키는 것으로 나타났다. 기전적으로, 메트포르민은 티오레독신-상호작용 단백질(TXNIP)의 발현을 감소시켜 포도당 수송체 1(GLUT1)의 발현과 막 국소화를 증가시켰다. 장 내 TXNIP 과발현은 당뇨병 모델 마우스에서 메트포르민의 혈당 강하 효과를 소멸시켰으며, GLUT1 억제 역시 메트포르민의 혈당 강하 효과를 차단하였다. 또한, 메트포르민은 장 내에서 포도당 신생합성(glyconeogenesis)보다 해당작용(glycolysis)을 우선적으로 촉진하는 것으로 확인되었다. 본 연구는 메트포르민이 혈당을 낮추는 새로운 기전을 밝혀내어, 전통적인 당뇨병 치료를 넘어서는 치료적 가능성을 제시하였다.

핵심되는 말 : 포도당 항상성;메트포르민;포도당수송체단백질1;위장관경로; 티오레독신 상호작용 단백질;